Max Planck Institute
for Polymer Research

JOHANNES GUTENBERG
UNIVERSITÄT MAINZ

Microstructural Characterization of the Influence of Protein Corona on the Intracellular Transport of Drug Delivery Systems

Master Thesis

Submitted by

Yeliz Yangazoglu

Matriculation Number: 2731582

M. Sc. Biology, JGU

Submitted on 15.10.2019

1. Supervisor: Prof. Dr. Katharina Landfester & Dr. Ingo Lieberwirth

Max Planck Institute for Polymer Research, Germany

2. Supervisor: Prof. Dr. Thomas Hankeln

Johannes Gutenberg University, Germany

DECLARATION OF AUTHORSHIP

Name: Yeliz Yangazoglu

Matriculation Number: 2731582

I hereby declare that this Master's Degree Thesis is entirely my own except where indicated by full references.

Signature: ..... Date: __/__/_____

1. Supervisor's Signature: ..... Date: __/__/_____

Signature: ..... Date: __/__/_____

2. Supervisor's Signature: ..... Date: __/__/_____

1. Supervisor: Prof. Dr. Katharina Landfester & Dr. Ingo Lieberwirth

2. Supervisor: Prof. Dr. Thomas Hankeln

Contents

Abbreviations	
CLEM	Correlative Light and Electron Microscopy
cLSM	Confocal Laser Scanning Microscopy
DAB	3,3′-Diaminobenzidin
DMEM	Dulbecco's Modified Eagle's Medium
FBS	Fetal Bovine Serum
HBSS	Hank's Balanced Salt Solution
HRP	Horseradish Peroxidase
GFP	Green Fluorescent
JGU	Johannes Gutenberg University
MPIP	Max Planck Institute for Polymer Research
NM	Nanomaterial
NP	Nano-particle
PBS	Phosphate Buffered Saline
PS-NPs	Polystyrene Nanoparticle
SEM	Scanning Electron Microscopy
SDS-PAGE	Sodium Dodecyl Sulfate–Polyacrylamide Gel Electrophoresis
STED	Stimulated Emission Depletion Microscopy
TEM	Transmission Electron Microscopy
QD	Quantum Dot
QNP	Quantum Nanoplatelet

1. Introduction

In recent years, due to their small size and advantageous properties, nanoparticles (NPs) have become an intensive area of biotechnological and biomedical research. In biomedical fields, NPs are used for tissue engineering, in magnetic resonance imaging (MRI) for contrast enhancement in tumor imaging and for drug delivery [1]. Several of these applications are already in clinical use. Different types of nanoparticles are used but generally biodegradable NPs, like polymer based nanoparticles and liposomes are preferred for drug delivery and targeting tumors, thus eliminating possible side effects due to retention of nanocarriers [2].

Although the increasing studies about NPs and their interaction with cells, there are still many unanswered questions. Therefore, to answer these questions, more studies should be done. For example, cytotoxicity, internalization studies using different NPs types to determine the internalization, damage and the cellular uptake mechanism of NPs. The internalization of NPs and their cellular uptake mechanism depends on the properties of the NPs like their size, surface chemistry or shape, but also on the cell physiology. Mechanistic understanding of endocytosis and intracellular trafficking of NPs is essential for designing new NPs and also to understand the utilization potential of the produced nanoparticles and nanocarriers.

To understand the fate and the pathway of NPs, the nanoparticle-cell interaction should be extensively visualized. To visualize intracellular nanoparticles, the commonly used microscopy systems are light microscopy e.g. confocal laser scanning microscopy (cLSM) or stimulated emission depletion microscopy (STED). In the field of electron microscopy imaging transmission electron microscopy (TEM) and scanning electron microscopy (SEM) are commonly used for imaging of cells with the internalized NPs. Optical microscopes are generally used for fluorescent labeled nanoparticles, and to visualize endocytotic pathways by using green fluorescent proteins (GFP) which is expressed by the cell as e.g. endosome proteins such as GFP-RAB5. However, any other fluorescent dye can be used for labelling cell compartments or the NPs themselves.

Electron microscopy is also used for NP research, mostly for NP characterization and analysis of surface characteristics. SEM is used for observation of morphological changes in cell membranes after incubation with NPs [3, 4]. On the other hand, TEM is

widely used for observation of internalized NPs inside cells or to determine the subcellular location of NPs and their aggregation [5-9]. But it is not always possible to obtain the desired information with a single microscopy method. In such cases, correlated light and electron microscopy (CLEM) techniques are required. These combine the power and advantages of the different imaging systems and are applied mostly on the identical specimen, which is prepared to perform for both, electron and optical imaging methods, simultaneously. Light microscopy offers the advantages of rapid screening of a large area of the sample, fast determination of labeling specificity and simultaneous detection of multiple antigens. Electron microscopy, on the other hand, provides the unique "reference space" where all objects (labeled and unlabeled) can be visually explored at high resolution, but they have only gray scale and do not contain information on the molecular level. In addition, there is no chance for live cell imaging with TEM or SEM. CLEM technique allow us not only to combine different microscopy systems, but also different stages of the sample preparation process, such as live cell imaging followed by cell fixation and subsequent EM imaging.

The aim of my master thesis is to visualize various NPs and nanocapsules in the intracellular environment including the visualization of the protein corona. The protein corona forms immediately, when a nanoparticle come into contact with plasma or any biological-fluids, which includes proteins. These contain proteins which will cover the surface of nanoparticles immediately and form a biological active protein corona. The effect of protein corona for the fate of the nanoparticles is as important as the effect of cell properties and size, surface characteristics, shape and chemistry of the NPs. Therefore, the structure of protein corona needs to be well investigated. During my master thesis studies, I incubated various NPs, including inorganic nanoparticles such as quantum platelets and organic nanoparticles such as protein nanocapsules to mouse macrophages (RAW 264.7 cell line) with different concentrations and incubation times. After that I visualized these nanoparticles in the intracellular environment by using different microscopic methods, cLSM (Correlative Light and Electron Microscopy), TEM (Transmission Electron Microscopy), SEM (Scanning Electron Microscopy) and CLEM (Correlative Light and Electron Microscopy) technique and I also briefly looked into the intracellular fate of internalized NPs and their effect of cells.

Firstly, I visualized quantum platelets, which are inorganic nanoparticles, in RAW 267.4 cells. Due to their unique optically properties, especially the high quantum yield,

it was quite easy to identify them in the intracellular environment, because they have very bright fluorescence and very high electron dense (it means they give very strong contrast in TEM visualizing). Then I tried to visualize nanocapsules composed of bovine serum albumin (BSA). These are protein nanocapsules and like other organic nanoparticles, it is very difficult to identify them in the cell because their shapes are very similar like other cell parts and they have very low electron dense; it means they give very poor contrast in TEM visualizing. Therefore, I used quantum platelets (because of their optical properties) as a marker in order to enhance the identification by means of TEM visualization of the BSA nanocapsules. In this way, they were easily detectable in the RAW 264.7 cells. Quantum platelets were good markers for TEM and fluorescent imaging, but it is difficult identify them by SEM imaging. Therefore, in a next step, I visualized hydroxy-ethyl starch (HES) nanocapsules labelled with Cy5 organic dye. As mentioned before, electron microscopes have only gray scale, so it is not possible to see any fluorescence of Cy5 organic dye, and due to the low resolution of confocal laser scanning microscopes the cLSM images were not informative enough. So I performed for HES nanocapsules CLEM technique by overlaying SEM and cLSM images from the same area. In this way, I identified and imaged HES nanocapsules in mouse macrophages. My next aim was to visualize HRP (Horseradish peroxidase) nanocapsules in the intracellular environment. As we know from many biochemical applications, HRP enzyme are commonly used with 3,3´-diaminobenzidine (DAB) and H_2O_2 as detection assay. After DAB staining, the HRP nanocapsules become black (the HRP enzyme catalyzes H_2O_2 and triggers the DAB reaction, DAB is oxidized and forms the very stable polybenzimidazole, which is obserable as a brown-black product). Using this staining method, the HRP capsules are easily detectable by cLSM and SEM. As mentioned before, the protein corona plays a very important role for the uptake and fate of the nanoparticles, so it is very important to get detailed information about it. Therefore, the final step in this master thesis is to visualize the protein corona by combining the methods developed before. The morphology of protein corona is not well understood and it not yet clear, in which way the protein corona is involved to the uptake process and the subsequent intracellular trafficking. To visualize the protein corona I used polystyrene nanoparticles (PS-COOH and PS-NH_2). PS-NPs were first incubated with Cy5 labeled mouse plasma then after formation of protein corona the PS-NPs were incubated to mouse macrophages. Then, using CLEM technique, I performed imaging of both polystyrene nanoparticles and Cy5 stained protein corona.

The visualizing of protein corona was successfully and was very promising for getting better knowledge about the role of the protein corona for the NP-cell interaction and their intracellular processing.

1.1. Nanomaterials

The definition of a nanomaterial is that at least one dimension is sized between 1 and 1000 nanometers [10]. However, common nanoparticles have dimensions between 10 and 500 nm. Although it is possible to classify nanoparticles according to many properties, we can roughly divide them into two classes, inorganic-based nanoparticles and organic-based nanoparticles. A nanoparticle usually forms the core of nano-biomaterial. It can be used as a convenient surface for molecular assembly and may be composed of inorganic or polymeric materials. It can also be in the form of nano-vesicle surrounded by a membrane or a layer. The shape is more often spherical but cylindrical, plate-like and other shapes are possible. The size and size distribution might be important in some cases, like for the cellular uptake of the nanoparticles. The size and size distribution are becoming extremely critical when quantum-sized effects are used to control material properties. A tight control of the average particle size and a narrow distribution of sizes allow creating very efficient fluorescent probes that emit light in a very wide range of wavelengths. This helps creating biomarkers with many and well distinguished colors. The core itself might have several layers and can be multifunctional. For example, combining magnetic and luminescent layers one can both detect and manipulate the particles.

The core particle is often protected by several monolayers of inert material, for example silica. Organic molecules, those are adsorbed or chemisorbed on the surface of the particle are also used for this purpose [11].

1.1.1 Visualizing Intracellular Nanoparticles

It is possible to classify nanoparticles in many ways. For examples; according to their morphology or according to their applications or elemental composition. According to their composition, we can divide nanoparticles into 2 classes; inorganic nanoparticles and organic nanoparticles. Inorganic nanoparticles typically include metal and metal oxides. Due to their optically properties they have high electron dense and thus give a good contrast for EM imaging. Some example of inorganic nanoparticles such as gold nanoparticles and quantum dots are shown in **Figure 1**. Organic nanoparticles such as polymer based nanoparticles and liposomes have some difficulties regarding their visualizing by TEM or SEM. Because their electron density is very similar to the surrounding resin, in which the cells usually are embedded for EM imaging, they suffer

from a very poor contrast and it is quite difficult to unambiguously identify them. Additionally, their shape is very similar to other cell compartments and structures, which appear to have a spherical shape as well. Therefore it is quite difficult to identify them in the intracellular environment.

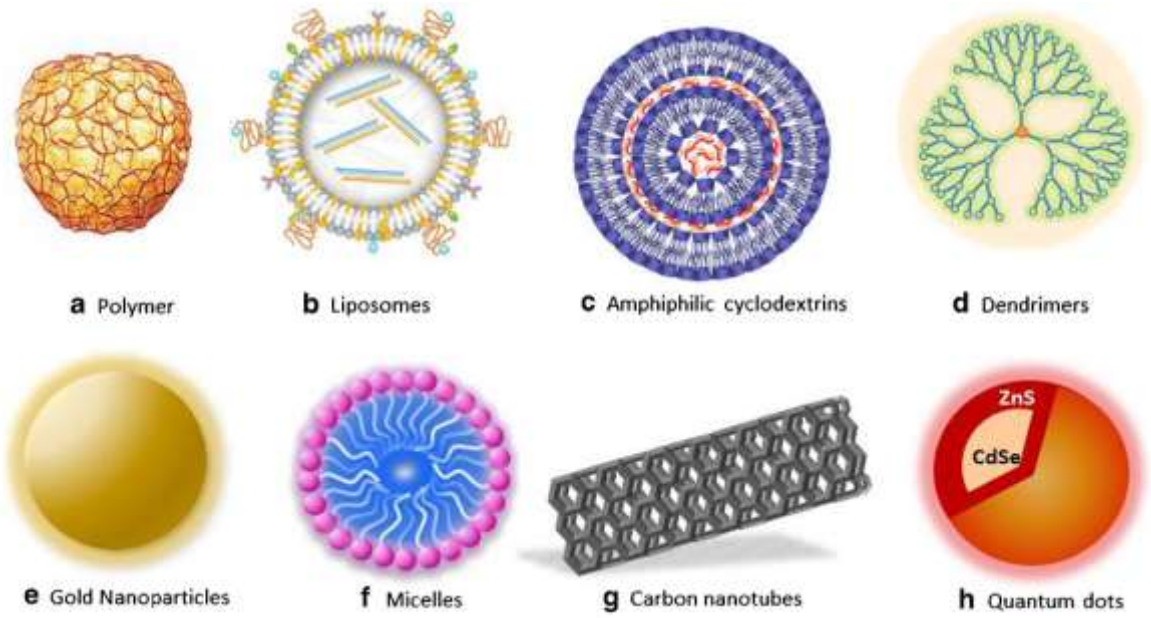

Figure 1: Examples of organic-based polymers; a. Polymer, b. Liposomes, c. Amphiphilic cyclodextrins, d. Dendrimers. Examples of inorganic-based nanoparticles: e. Gold nanoparticles, g. Carbon nanotubes, h. Quantum dots. Diagram taken form [11].

1.1.1.1 Inorganic-based Nanoparticles

Inorganic-based nanoparticles include metal and metal oxide NPs. They can be synthesized into metals such as Au or Ag NPs, metal oxides such as TiO2 and ZnO NPs, and semiconductors such as silicon and ceramics [12]. The cellular uptake of inorganic nanoparticles has been in focus of studies, because they are easily detectable in the cell by means of TEM studies. Inorganic nanoparticles can penetrate or interact with the organelle structures and due to their electron-dense appearance in TEM, they can be well observed in the intracellular environment or at the extracellular membrane [13]. The fate of nanoparticles in the cell depends on many factors like their size [14, 15], shape [14, 16], aggregation state [17], surface charge [18], crystalline state [19, 20, and 21] and their tendency to form a protein corona [22]. The studies were generally focused on the uptake of medium and small size nanoparticles [23]. For example

Hillyer and Albrecht [24] compared the uptake of 4, 10, 28 and 58 nm gold nanoparticles in the GIT (Gastrointestinal Tract) tissue of mice by quantitative transmission electron microscope investigations. They have found that smaller particles crossed the GIT more easily than the larger ones and they explained that the passage from the intestine takes place through a persorption mechanism. It was also found that particle size has a significant effect on toxicity of the NP system and a study of Yu et. al. [25] supported it. Yu et. al. investigated the uptake of various size of silica particles (30, 48, 118, 535 nm) into HEL-9 (mouse keratinocytes). By TEM investigations it was found that all silica nanoparticles were internalized into vesicular structures inside the cytoplasm. They also performed mitochondrial viability assays as well as lactate dehydrogenase to measure the cytotoxicities of nanoparticles. Their findings showed that the small particles (30, 48 nm) were clustered within the vesicular structures inside the cells, the large 535 nm particles were taken up as individual particles and the small particles induced cytotoxicity associated with apoptosis, at higher concentrations, even result in chromosomal damage along with proinflamattory effects. On the contrary, these adverse effects were not observed for larger nanoparticles. In many publications, the effect of nanoparticles on cell uptake was masked by other effects, like formation of aggregates. The aggregate size dominates the uptake characteristic rather than the size of individual nanoparticle. Aggregates with a size below 200 nm stimulated membrane responses characteristic for a clathrin-mediated uptake and the uptake of larger particle clusters is attributed to a micropinocytosis (Calero et. al.). Another important factor, which effect the uptake, is the formation of a protein corona. In the in vitro studies with nanoparticles, the cell culture media can directly interact with the nanoparticles [26, 27]. These interactions affect the particles integrity and particle aggregation as a result of charge shielding by the high salt concentrations of the media. The cell media also contains a plurality of serum proteins, resulting in the formation of a protein corona on the surface of the nanoparticles. The formation of protein corona entails several implications on the biological activity of the NP systems like the cytotoxicity or immunotoxic effects [28].

The effect of protein corona on particle stabilization remains controversial and sometimes conflicting results appear in the literature. As an example, citrate-stabilized AuNPs (gold nanoparticles) have been reported to be colloidal stabilized in the presence of protein [30], but have also been reported to undergo aggregation in protein-

containing growth medium. In many instances, incubation of citrate-stabilized AuNPs, including fetal bovine serum (FBS), has been proven by a number of different physicochemical methods, results in the increase of particle size and in the occurrence of particle aggregates [31, 32, 33]. TEM imaging has shown for cells exposed to AuNPs in a serum-containing cell medium the occurrence of large nanoparticle aggregates inside or outside the cells. The particles were observed as aggregated structures within vesicular structures. It is unsurprising that the presence of protein corona also has a strong effect on the uptake mechanism; therefore, it is unsurprising that, for example, caveolae-mediated, clathrin-mediated, or macropinocytic uptake of AuNPs in serum medium could be observed, which points toward the stimulation of active uptake mechanisms.

1.1.1.2 Organic-based Nanoparticles

Organic-based nanoparticles like polymeric nanoparticles basically consist of the elements with cell like carbon, hydrogen, oxygen, nitrogen etc. Scientific studies on polymeric nanoparticles have been increasing in recent years. However, it is quite difficult to visualize them by electron microscopy compared to inorganic nanoparticles.

Polymeric nanoparticles are organic-based and colloidal nanoparticles of size range 10 nm–1 μm and solid in nature. They can be made of biodegradable and biocompatible polymers or copolymers, in which the drug can be entrapped or encapsulated within the carrier, physically adsorbed on the surface of the carrier or chemically linked to the surface [34]. The use of polymeric nanoparticles as vehicles for drug delivery applications has gained increasing attention recently and the field encountered tremendous interest [35]. In cancer studies, targeted polymeric NPs can be used to deliver chemotherapies to tumor cells with greater efficacy and reduced cytotoxicity on peripheral healthy tissues [36]. This is related to their excellent endocytosis efficiency, passive and active tumor targeting, and the possibility of encapsulating a wide range of therapeutic agents with high encapsulation efficiency. Polymeric nanoparticles can consist of many different monomer variations. This allows them to change many of their properties through engineering applications. For example, by defining their size, shape, surface, and even target units to control their interaction.

Polymeric nanoparticles are used for different formulations of drugs by using one of these methods, including, adsorption, dissolution, entrapment, encapsulation or

chemical binding of drug molecules on the surface of polymeric nanoparticles. The drug release kinetics and its characteristics solely depend on the drug trapping method and polymer structure [37]. The use of biodegradable polymeric nanoparticles (NPs) for controlled drug delivery has demonstrated significant therapeutic potential. In cancer, targeted polymeric NPs can be used to deliver chemotherapies to tumor cells with more effective and reduced cytotoxicity in peripheral healthy tissues. This is promising to eliminate many problems in cancer treatments.

Polystyrene (PS) is one of the most commonly used polymers. Its molecular structure with aromatic chains makes it hardly biodegradable. It is used in food packing, pharmaceuticals, as container materials of cosmetics etc. The surface charge properties of PS nanoparticles can be controlled by the use of polymers as surfactants having amino ($-NH_2$) or carboxy (-COOH) functionalities during the emulsion process. They can also be used for instance to attach fluorescent dyes to the particle surface. So they can be used for cLSM visualization. A lot of studies showed that the PS NPs don't participate in the staining process and appear with bright contrast by TEM imaging, in other words the PS NPs are stable toward the standard embedding protocol and appear with a bright TEM contrast owing to reduced electron density compared to the background [38, 39, and 40].

Another form of the nanocarriers are nanocapsules. For cellular uptake, the nanocarriers have to be preferably smaller than 300 nm. Nanocapsules can deliver a high amount of therapeutic molecules. For the formation of stable polymeric nanocapsules with an aqueous core, the inverse miniemulsion has been shown to be a very versatile technique that also allows the use of polymers and biomolecules for the shell formation [41].

HES is a hydroxyethylated glucose polymer that is used in medicine for the treatment of hypovolemic shock, artery occlusive disease, cerebral ischemia or apoplectic insult, respectively. HES improves the microcirculation within the organism, due to the improvement of blood viscosity [42, 43, and 44], In principle, polymeric HES particles or capsules are very suitable for the encapsulation of various biomolecules due to the biological tolerance and degradability, shelf life, high loading capacity and the possibility of a targeted release [45].

1.2. Correlative Light and Electron Microscopy (CLEM)

It is not always possible to obtain all the desired information with a single microscopy method. Although light microscopy offers the rapid screening of a large area of the sample at relatively low resolution, fast determination of labeling specificity, and the simultaneous detection of multiple antigens by live-cell imaging, EM provides the unique "reference space" where all objects (labeled and unlabeled) can be visually explored at the highest resolution. The most-informative approach would be the convergence of these two types of microscopes, allowing direct correlation of the data sets obtained from one sample [46].

In the case of correlative light and electron microscopy, spatial and structural data are combined to determine the interactions of cellular components, primarily in living systems [47]. Fluorescence light microscopy (FM) or confocal laser scanning microscopy (cLSM) utilizes fluorescent signals or markers to image the interactions, and electron microscopy on the other hand, can reveal ultrastructural details of cellular architectures beyond the limit of optical resolution [48].

In other words; correlative microscopy combines the power and advantages of different imaging systems (light, electron, X-ray, NMR, etc.), such as confocal laser scanning microscopy (cLSM), super-resolution microscopy (SFM), transmission electron microscopy (TEM) and scanning electron microscopy (SEM), atomic force microscopy (AFM), magnetic resonance imaging (MRI), superconducting quantum interference devices (SQUIDs), and in vivo imaging (IVIS@) containing micro/nano CT (computed tomography). This technique can be applied not only to different imaging systems, but also to different stages of sample preparation process; such as live specimen and fixed specimen [49].

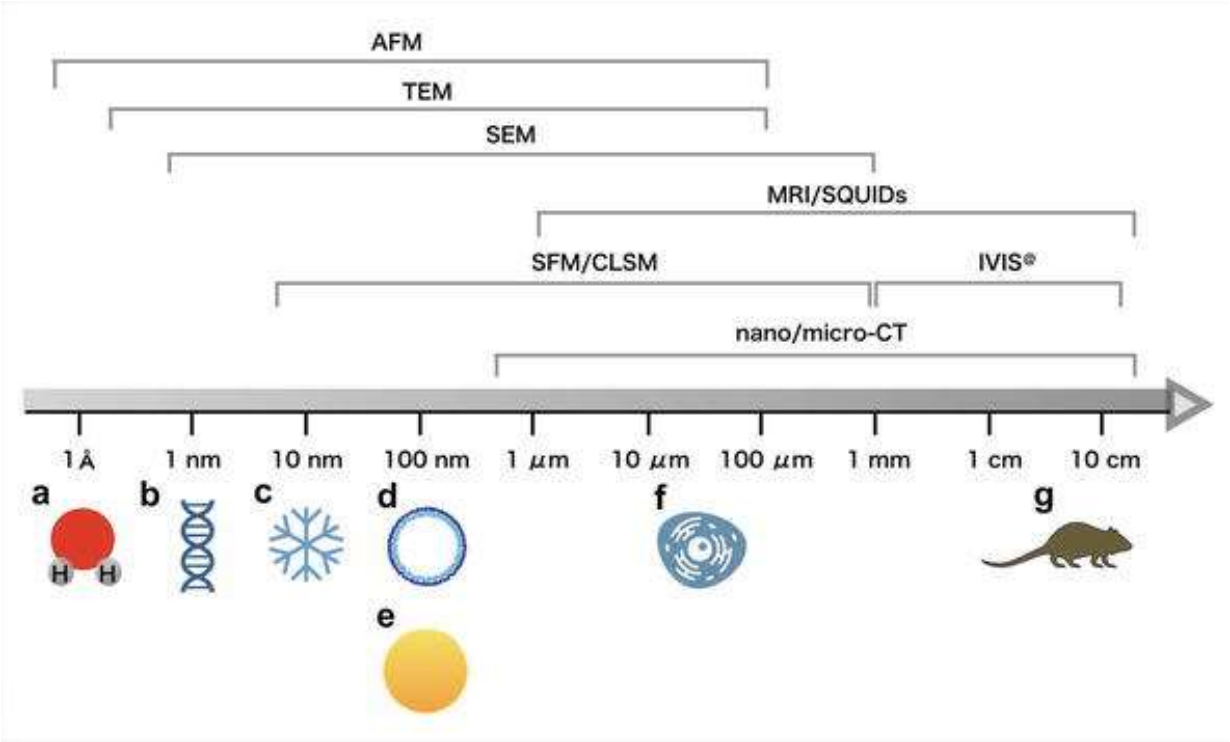

Figure 2: Scale-based representative objects and corresponding microscopic tools for CLEM imaging: atomic force microscopy (AFM), transmission electron microscopy (TEM) and scanning electron microscopy (SEM), magnetic resonance imaging (MRI), superconducting quantum interference devices (SQUIDs), confocal laser scanning microscopy (cLSM), super-resolution microscopy (SFM), and in vivo imaging (IVIS@) containing micro/nano CT (computed tomography). (a) H2O, water molecule (~2 Å), (b) DNA double helix (2–10 nm), (c) dendrimer (1–10 nm), (d) liposome (50–500 nm), (e) gold particle (50–200 nm), (f) cell (5–50 μm), and (g) a mouse (2–10 cm). Diagram is taken from [45].

1.3 Protein Corona

When the nanoparticles come into contact with plasma or other protein-containing biological fluids, the surface of the nanoparticles is immediately surrounded by proteins that form a biologically active protein corona. The biological fate and function of nanoparticles is determined by physiological responses to these nanoparticle-protein corona complexes as the effective biological unit of nanoparticles [50].

The protein corona is divided into two layers: an inner constant layer, the so-called hard corona, and an outer dynamic soft corona [51]. Forming the hard corona are proteins with strong binding affinity to the surface of nanoparticles, have longer surface residence time and are in higher abundance relative to the other protein members of the

corona. Often, the plasma proteins immunoglobulin and apolipoprotein are found in the hard corona of various types of nanoparticles [52]. The soft corona, on the other hand, is the ‘external corona’ composed of weakly bound proteins, such as the plasma protein albumin, with shorter surface residence time and lower abundance in the corona relative to the other protein members of the corona. In rapid equilibrium with the ‘free’ proteins in the biological fluid, the soft corona is sensitive to changes in the protein profile of the biological fluid and dissociates quickly upon decreasing concentrations of the ‘free’ proteins. Interestingly, it has been frequently observed that the major proteins in the plasma or other body fluids are not the most abundant proteins in the hard corona. Corona proteins are in fact enriched or depleted relative to their physiological abundance in the biological fluids. For example, proteins such as albumin and transferrin are often detected in very low concentrations in the hard corona despite their rich presence in the plasma. Alternatively, due to preferential interactions of nanoparticles with specific proteins, the particles can act as concentrator for the proteins, despite their low abundance in the plasma. As a result, the corona's protein patterns significantly differ from that of the plasma [53]. It is assumed that the proteins of the hard corona are directly linked to the NC surface, while the soft protein corona is only weakly linked to the hard corona via protein-protein interaction. As a result, the hard corona is expected to stay on the NPs even after the uptake into the cell via endocytosis, whereas the soft corona is lost [54].

The adsorption of proteins on nanoparticles (NPs) can modify the diverse physicochemical properties of NPs such as size, surface charge, surface composition and functionality, hence giving NPs a new biological identity. This NP–protein complex, not bare NP, determines various biological responses such as fibrillation, cellular uptake, circulation time, bioavailability and even toxicity. The layers consisting of bound or adsorbed proteins around NPs are called the protein corona. High surface energy may enhance the binding of protein on to the surface.

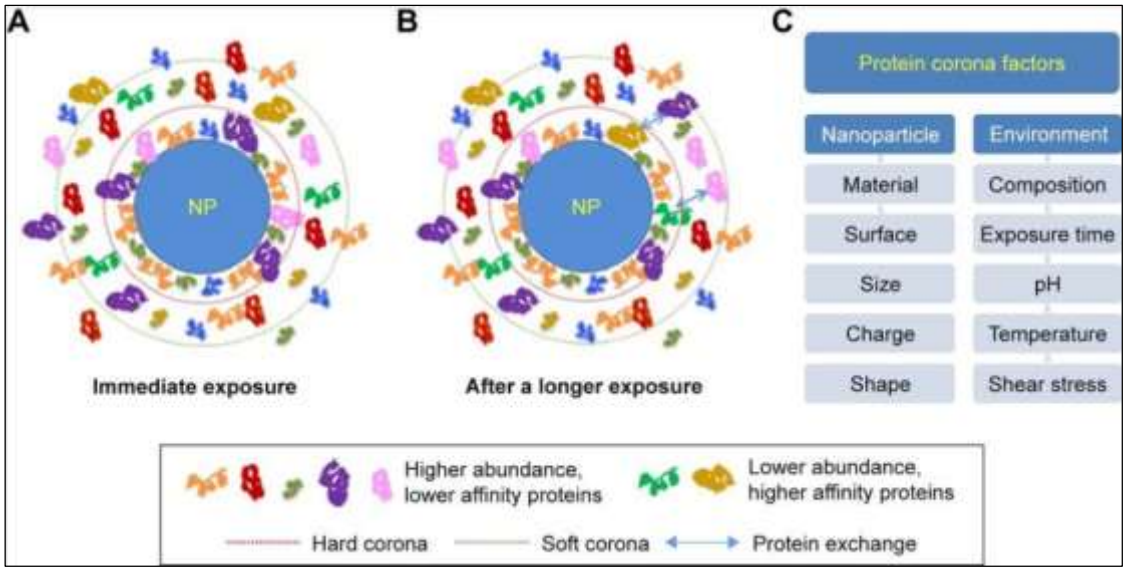

Figure 3: The formation of protein corona and exchange of adsorbed proteins over time in biological conditions. (**A**) Immediately upon exposure. (**B**) After a longer exposure time, with displacement of proteins among the hard corona, soft corona, and cellular environment. (**C**) Major factors affecting protein corona pattern divided into two categorized properties: nanoparticle and environment. Diagram is taken from [55].

The protein corona significantly influences the properties of the particles and their interaction with their environment [56]. The protein adsorption depends on the surface composition of the NP and leads to a change in size, electrical charge and surface functionalization, thus having a major influence on the interaction between particles and cells [57]. There are already different strategies to reduce non-specific protein adsorption via surface functionalization and as a result, the interaction between particles and cells can be better influenced [58, 59]. The effect of opsonization described by Owens and Peppas and the subsequent recognition and uptake of the particles by phagocytic cells of the immune system plays a central role. Opsonins are proteins that facilitate the adhesion of phagocytic cells to foreign cells or particles by attaching themselves to the target structure and thus marking them [60]. The camouflage is therefore particularly valid for the body's own immune system, which enormously decimates the half-life of uncamouflaged particles in the blood circulation and instead of accumulating in the target tissue results in their accumulation in the liver and spleen [61]. One method to achieve the stealth effect is to modify the NC surface with PEG. This so-called "PEGylation" is currently also the most common form of such functionalization [58], but is not optimally suited for clinical applications due to its lack

of biodegradability. For this reason, the establishment of biodegradable alternatives, such as polyphosphates, is an important part of current research [43].

1.4 Aim of This Study

The objective of this study is to visualize the interaction of the cell with nanoparticles; like intracellular uptake of NPs, their localization in the cell, their intracellular transporting mechanism etc. Imaging the nanoparticle-cell interaction is an important step in terms of understanding the utilization potential of these nanoparticles in bio-medicine and to get the required knowledge to designing / developing new nanoparticles. Moreover, the final goal of this thesis is to unambiguously identify polymeric nanoparticles together with the protein corona in a cellular environment by using CLEM methods.

I visualized this interaction with different suitable techniques like cLSM, TEM, SEM imaging or CLEM technique. Inorganic nanoparticles were very easy to visualize in RAW 264.7 cells. But because of their low electron dense and similarities to other structures in the cell, imaging of organic nanoparticles was more arduous. I have applied different methods to facilitate / enable imaging of these organic nanoparticles. For example, I visualized HRP nanocapsules with DAB staining, the BSA nanocapsules by using quantum nanoplatelets as marker. I also applied CLEM technique for HES capsules by using Cy5 organic dye. In this way, I gained in-depth knowledge of the interaction of the cell with nanoparticles by gaining experience in many imaging techniques during the thesis process.

After applying all these techniques and obtaining sufficient accumulation, the main purpose of my thesis was to select and apply the most appropriate method that can provide imaging of protein corona.

In recent years, studies on protein corona have increased gradually. However, the studies to display the morphology of biological active protein corona are quite insufficient. Therefore I also focused on visualizing protein corona by using Cy5 organic dye. I preferred Cy5 dye to visualize the protein corona, because many organic dyes can’t survive EM sample preparation process, but Cy5 dye does. I performed this experiment by using green fluorescent polystyrene nanoparticles. So it was easier to define the protein corona’s shapes and borders.

2. Materials and Methods

2.1 Cell Cultivation

Product	Provider
DMEM	Life technologies™; Grand Island; NY USA
FBS	Life Technologies GmbH; Darmstadt; Deutschland
GlutaMAX™-I	Life technologies™; Grand Island, NY; USA
Cell Scraper	Nunc™, Thermo Scientific™, USA
0,25 % Trypsin/EDTA	Life technologies™; Grand Island; NY USA
PBS	Life technologies™; Grand Island; NY USA
Trypanblue	SIGMA®; Steinheim; Deutschland

Table 1: Cell Line Materials used for cell growth and sample preparation and respective provider

2.1.1 Cell Medium

The medium used for cell cultivation was Dulbecco's modified eagle medium(DMEM) supplemented with 10% fetal bovine serum (FBS), 100 IU/ml Penicillin, 100 µg/ml Streptomycin and 1% GlutaMAX.

2.1.2 Cell Cultivation

In this thesis, RAW 264.7 cells (Mouse macrophage cell line, CLS; Eppelheim; Deutschland) were used for all experiments. The cells were cultivated in 75cm^2 cell culturing flasks with 15mL DMEM, incubated at 37°C with 5% CO_2 and kept in the exponential growth phase. 1-2 million cells were transferred to the new flask, splitting was done every third or fourth day. The cells were split by removing the medium and gently washed with 10 mL sterile phosphate buffered saline (PBS, Sigma Aldrich). PBS was then removed and 3 mL of 0.25% trypsin and 0.2% EDTA (Sigma Aldrich) was added to detach the cells from the incubation flask. The trypsin was allowed to work for 5 minutes at 37°C before the trypsination was stopped by adding 8 mL cell medium to the flask. This mix was added to a Falcon tube and centrifuged at 500 rcf for 5 minutes. After centrifugation, the cells were resuspended in 3 mL DMEM. The

concentration of living cells was then analyzed using a cell counter slides by mixing 20 µL of the solution and 20 µL trypan blue. Then the cells are diluted and 1-2 million cells were passaged to a new flask. The remaining cells were either used for experiments or discarded. Back up of cells in case of infection was done either by cooperation with others working with the same cell line, or by keeping a second flask of cells. During the cultivation of cells, the medium was normally changed once during every passage.

Equipment	Provider
Vortexer	Heidolph; Schwabach; Deutschland
HERAEUS PICO 21 Centrifuge	Thermo Scientific; Waltham; MA USA
Centrifuge 5810R/5804R	Eppendorf; Wesseling-Berzdorf; Deutschland
Cell Counter	Bio-Rad Laboratories. USA
Waterbad	Memmert; Schwabach; Deutschland
Inkubator C200	Labotect; Rosdorf; Deutschland
Sterilbank C-[MaxPro]3-130	Berner FlowSafe®;Künzelsau;Deutschland
Sterilbank s@femate 1.2	BIOAIR®; Vorhees Township; NJ USA
Mikroskop CKX41	Olympus; Hamburg; Deutschland
FEI Tecnai F20 TEM	Thermo-fisher Scientific; Waltham; MA USA
Leica SP5-STED confocal Laser scanning microscope	Leica Microsystems; Wetzlar; Germany
Luminescent Image Analyzer LAS-3000	Fujifilm; Tokyo; Japan
Ultramicrotome	Leica EM UC7, Wetzlar, Germany

Table 2: Equipments for cell culture process and microscopes; and respective provider

2.2 Incubation with Nanoparticles

2.2.1 Incubation with Quantum Nanoplatelets

2.2.1.1 HHA 397-Ligand Exchange Nanoplatelet (Henry Halim, MPIP)

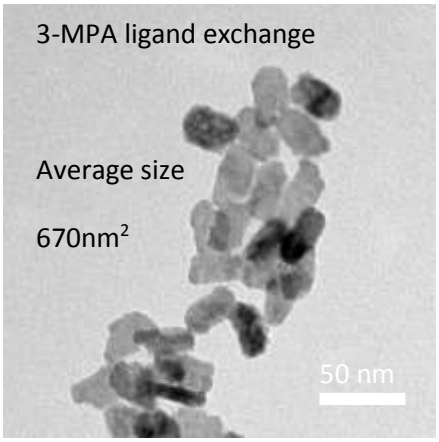

Figure 4: TEM image of free HHA 397- Ligand Exchange Nanoplatelets

The initial concentration of the HHA397 nanoplatelet was 10mg / mL. 2 solutions which containing different amount of nanoplatelet (18,75µg/mL and 75µg/mL) were prepared by diluting with cell media. The nanoplatelets are 2D CdTe quantumdots which have an extraordinary quantum yield. Accordingly, their fluorescence performance is very good and they can be easily localized by fluorescence imaging. Their morphology is platelettlike with an average size of 30 nm, as shown in Figure 4.

For incubation, RAW 264.7 cells were seeded out with a concentration of 500.00cells/mL in a 24-well plate (Greiner, Germany) containing three surface C-coated sapphire disks. The cells were adhered for 24 h on the sapphire discs. After 24 h, the HHA397 quantum platelets were added at a concentration of 75 µg/mL and 18,75 µg/mL to the cell medium and incubated for 1 h and 24 h at 37°C with 5% CO_2.

2.2.1.2 HHA296- Polymer Coated Nanoplatelet (CdZn QDs) (Henry Halim, MPIP)

The initial concentration of the HHA296 nanoplatelet was 10mg / mL. 2 solutions which containing different amount of nanoplatelet (18,75µg/mL and 75µg/mL) were prepared by diluting with cell media. An image of their morphology is shown in the TEM micrograph in **Figure 5**.

For incubation, RAW 264.7 cells were seeded out with a concentration of 500.000cells/mL in a 24-well plate (Greiner, Germany) containing three surface C-

coated sapphire disks. The cells were adhered for 24 h on the sapphire discs. After 24 h, the HHA296 quantum platelets were added at a concentration of 75 µg/mL and 18,75 µg/mL to the cell medium and incubated for 1 h and 24 h at 37°C with 5% CO_2.

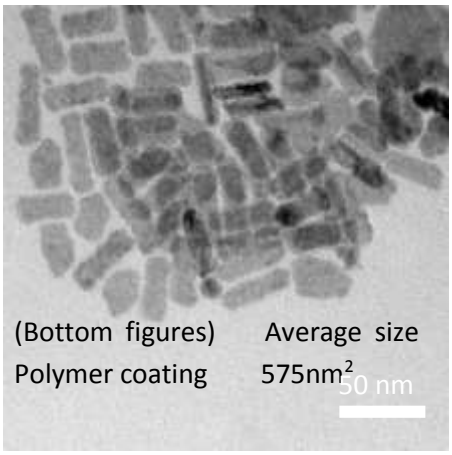

Figure 5: TEM image of free HHA296 – Polymer coated Nanoplatelets

2.2.2 Incubation with Nanocapsules

2.2.2.1 BSA Encapsulated Nanoplatelets HH242 & HES Encapsulated QNPs HH242

(HES Nanocapsules are also Cy5 labeled)

For preparation, the RAW 264.7 cells were seeded out with a concentration of 500.000 cells/mL in a 24-well plate (Greiner, Germany) containing three C-coated sapphire disks, and adhered for 24 h on the sapphire discs. BSA nanocapsules with HH242 quantum platelets were added at a concentration of 300 µg/mL and HES nanocapsules with Cy5 dye were added at a concentration of 300 µg/mL to the cell medium and incubated for 24 h.

	MF-106-BSA	**MF-106-HES**
Nanocapsules material	BSA	HES
Encapsulation	Nanoplatelets (HH242)	Nanoplatelets (HH242)
Concentration	10 mg/mL	10 mg/mL
Diameter	361 nm	617 nm
Zeta Potential	-28 mV	-18 mV

Table 4: Encapsulated Nanoplatelet and some of their properties. The size of the nanocapsules was determined by dynamic light scattering and the Zeta Potention using Zetasizer nano (R) (Malvern Instruments).

2.2.2.2 HRP Capsules + Cy5

For TEM Preparation: The RAW 264.7 cells were seeded out with a concentration of 500.000 cells/mL in a 24-well plate (Greiner, Germany) containing three , surface C-coated sapphire disks and adhered for 24 h on the sapphire discs. HRP Capsules with Cy5 were added at a concentration of 75 µg/mL to the cell medium and incubated for 1 h, 4h and 24 h (for 4h and 24 h the cell medium which contains HRP capsules were removed after 2 h and were added fresh cell medium to the wells).

For cLSM Preparation: The RAW 264.7 cells were seeded in µ-Dish 35 mm Imaging Chamber dishes. The remaining cell solution from splitting was diluted to a concentration of 20.000cells/mL. 1 mL (20.000 cells) was added to dishes and adhered for 24 h. HRP capsules with Cy5 were added at a concentration of 75 µg/mL to the cell medium and incubated for 1h, 4h, 24 h and for 48 h (for 4 h, 24 h and for 48 h the cell medium which contains HRP capsules were removed after 2 h and were added fresh cell medium to the dishes).

2.2.3 Polystyrene Nanoparticles (PS-COOH & PS-NH_2) + Cy5 labeled Protein Corona

	PS-COOH (KK90a)	**PS-NH_2 (KK91)**
Material	Polystyrene	Polystyrene
Surfactant	Lutensol	Lutensol
Concentration	10 mg/mL	10 mg/mL
Diameter	116 nm	126 nm
Zeta Potential	-7 mV	+ 7 mV

Table 5: PS-COOH (KK90a) & PS-NH_2 (KK91) +Protein corona Cy5

Cy5 Mouseplasma preparation:

1.4 mg NHS-Cy5 was incubated with 1.6 mL Mouseplasma for 1 h at room temperature, and then free Cy5 organic dye was removed by using 7kDa spin columns.

Coating of nanoparticles with Cy5-Mouseplasma:

~ 100 µl (0.05 m2) nanoparticle was incubated with 1 mL of Cy5 Mouseplasma for 1h at room temperature. After 1 h it was centrifuged with 20.000 g for 30 minutes. The supernatant was removed and the PS-NPs with Cy5 labeled mouse plasma was resuspend with ~ 100 µl of water.

For incubation, RAW 264.7 cells were seeded out with a concentration of 500.000cells/mL in a 24-well plate (Greiner, Germany) containing three surface C-coated sapphire disks. The cells were adhered for 24 h on the sapphire discs. After 24 h, PS-COOH (KK90a)+Cy5 labeled protein corona was added at a concentration of 150 µg/mL to the cells and incubated for 2 h and 24 h at 37°C with 5% CO_2. PS-NH_2 (KK91) was added at a concentration of 150µg/mL to the 24 h before seeded RAW 264.7 cells and incubated for 2h.

2.3 TEM (Transmission Electron Microscopy) Sample Preparation

At the specified residence times, the sapphire disks were removed from the wells and dipped into 1-hexadecane to remove the remaining medium. The disks were covered with aluminum disks to prevent squeezing of the cells and the sandwich was injected into a high pressure freezing device (Wohlwend HPF compact 02, Switzerland). The frozen sandwich was stored in liquid nitrogen.

The aluminum cover was removed in a liquid N_2 environment and the sapphire disk was transferred into anhydrous acetone at −90 °C, (Merck, Germany) containing 4% aqueous osmium tetroxide (Roth, Germany) and 0.1% uranyl acetate (Merck, Germany) as a freeze substitution (Leica EM AFS2, Germany).

The samples were slowly warmed to 0 °C over a time period of 18–20 h. After 1 h the freeze-substitution samples were warmed to room temperature, then the substitution medium was removed and the disks were washed 3 times with acetone at half hour intervals. Then the discs were incubated each for 1 hour in 1:2 EPON®-Acetone, in 1:2 EPON®-Acetone and in 2:1 EPON®-Acetone finally in 100% EPON® solution (epoxide resin, Fluka, Switzerland). After that the 100% EPON® were changed with fresh 100% EPON® solution and left overnight.

The next day, infiltration was completed and the disks were transferred into a new 1.5 mL reaction tube containing fresh 100% EPON® and arranged with the cell covered site to the vessel opening. The tubes were left in a furnace at a temperature of 60 °C for 3 days to polymerize the epoxide resin. The hardened samples were quickly cooled down with liquid N2, in order to break the resin block at the interface to the disk. The cells were then enclosed in the resin block. The block was divided in halves, then trimmed into a trapezoid area with an abundant number of cells, and then fixed in the ultra-microtome (Leica Ultracut UCT). With a diamond knife (Diatome Ultra, Switzerland), 60 nm thick sections were achieved and applied on a copper grid (3.05, 300 mesh, Agar Scientific, U.K.).

The sections were observed using a FEI Tecnai F20 transmission electron microscope operated at an acceleration voltage of 200 kV. Micrographs were taken on a Gatan US1000 2k slow scan CCD camera.

2.4 Confocal Light Electron Microscopy (cLSM) Sample Preparation

2.4.1 Chemical Fixation

Chemical fixation was performed with 4% Paraformaldehyde or 4% Glutaraldehyde for 10 minutes at room temperature.

For chemical fixation the cell culture medium was removed. The cells were washed with PBS to remove the excess protein derived from the culture medium and flood with 4% fixative in buffer. After 10 minutes the fixative was removed and the cells were washed again with PBS for 2-3 times.

2.4.2 DAB (3,3′-Diaminobenzidine) Staining for HRP Capsules

The DAB/Cobalt and Urea Hydrogen Peroxide Tablets (Sigma-Aldrich, Germany) tablets were taken from freezer and were allowed to reach room temperature. Then the tablets were dropped into an appropriate container. The container was filled with 5 mL ultrapure water and vortexed until the tablets dissolved. (The DAB staining solution was used within 15 minutes.)

The solution was added to the chemically fixed and with PBS washed cells (1 h. 4 h, 24 h) and stained for 4 minutes. After staining the staining solution was removed and the cells were washed 2-3 times with PBS.

Pierce™ DAB Substrate Kit (Thermo Scientific™) was also used for HRP capsules. For 5 mL reagents, 4,5 mL Stable Peroxide Substrate Buffer and 0,5 mL DAB Substrate (10X) were mixed and added to pre-fixed cells (for 48 h) which includes HRP nanocapsules. The DAB staining was performed for 5-7 minutes at 37°C.

2.4.3 Nucleus Staining

Pre-fixed cells were washed 2-3 times with HBSS (Hanks' Balanced Salt Solution). SYTOX™ Green Nucleic Acid Stain - 5 mM Solution in DMSO (Thermofisher Scientific, Germany) was diluted in HBSS to 1:30.000 and added to the cells. The SYTOX™ Green dye was incubated for 15 minutes at room temperature. After 15 minutes the cells were washed 2 times with HBSS.

2.4.4 cLSM Visualizing

The images for the intracellular localization of the particles were taken using a commercial setup (LSM SP5 STED Leica laser scanning confocal microscope, Leica, Olympus, Germany), consisting of an inverse fluorescence microscope (DMI 6000 CS) equipped with a multi-laser combination, in addition to five detectors operating in the range of 400–800 nm. An HCX PL APO CS 63×/1.4–0.6 oil-immersion objective was used in these studies. Fluorescent particles were detected at 625-670 nm, which corresponds to red in color. The nucleus was stained with SYTOX™ Green Nucleic Acid Stain - 5 mM Solution in DMSO (Thermofisher, Germany) and appears as a green color (detected at 504-523 nm).

2.5 Cell-Viability Test

For testing the cell toxicity, I used the the CellTiter-Glo® Luminescent Cell Viability Assay.The cells were seeded into 96-well-plate (Greiner 96 Flat Bottom White Polystyrene); 10.000 cells/100µL/well and adhered overnight. HRP nanocapsules were added with concentrations of 30µg/mL, 60µg/mL and 120µg/mL and incubated for 6 h and 30 minutes. Reagent was prepared as manufacturer information and added to each wells with 100µL volume and the luminescence was measured by Tecnai-i-control luminescence microplate reader.

3. Results and Discussion

3.1. Visualizing Intracellular Quantum Nanoplatelets

3.1.1 HHA397 Nanoplatelets (Henry Halim, MPIP)

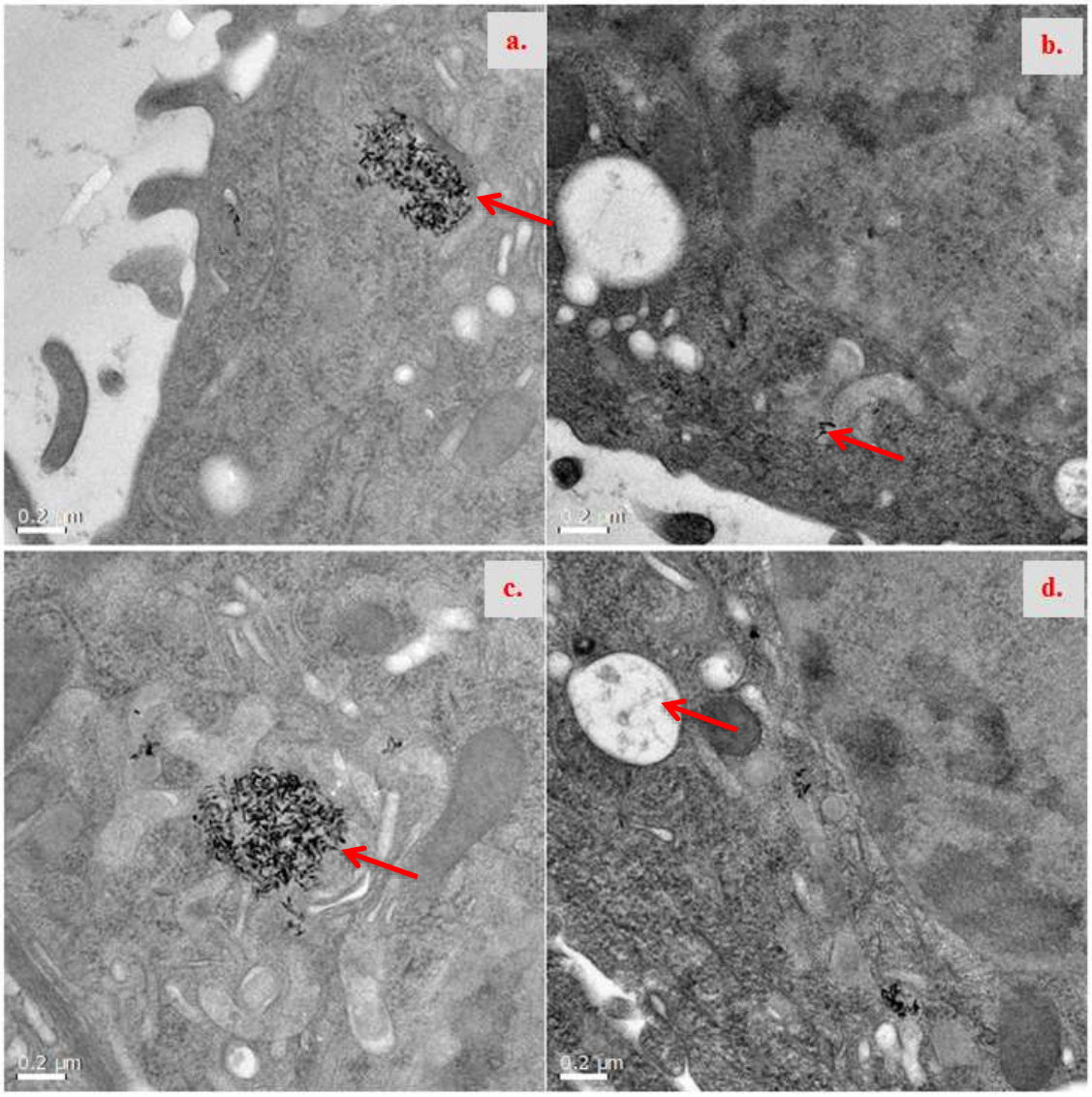

Figure 6: TEM Images of the cellular uptake and intercellular localization of HHA397 NPs with a concentration of 75 µg/mL for 24 h (the cells were washed after 1 h with PBS and added fresh cell growth medium without NPs, and incubated another 23 h) ***a)*** *HHA397 NPs in RAW 264.7 cells in endosome/lysosome vesicle, scale 200 nm* ***b)*** *HHA397 NPs in RAW 264.7 cells, scale 200 nm* ***c)*** *HHA397 NPs in RAW 264.7 cells in cluster, scale 100 nm* ***d)*** *Probably protein corona associated to several NPs, scale 500 nm*

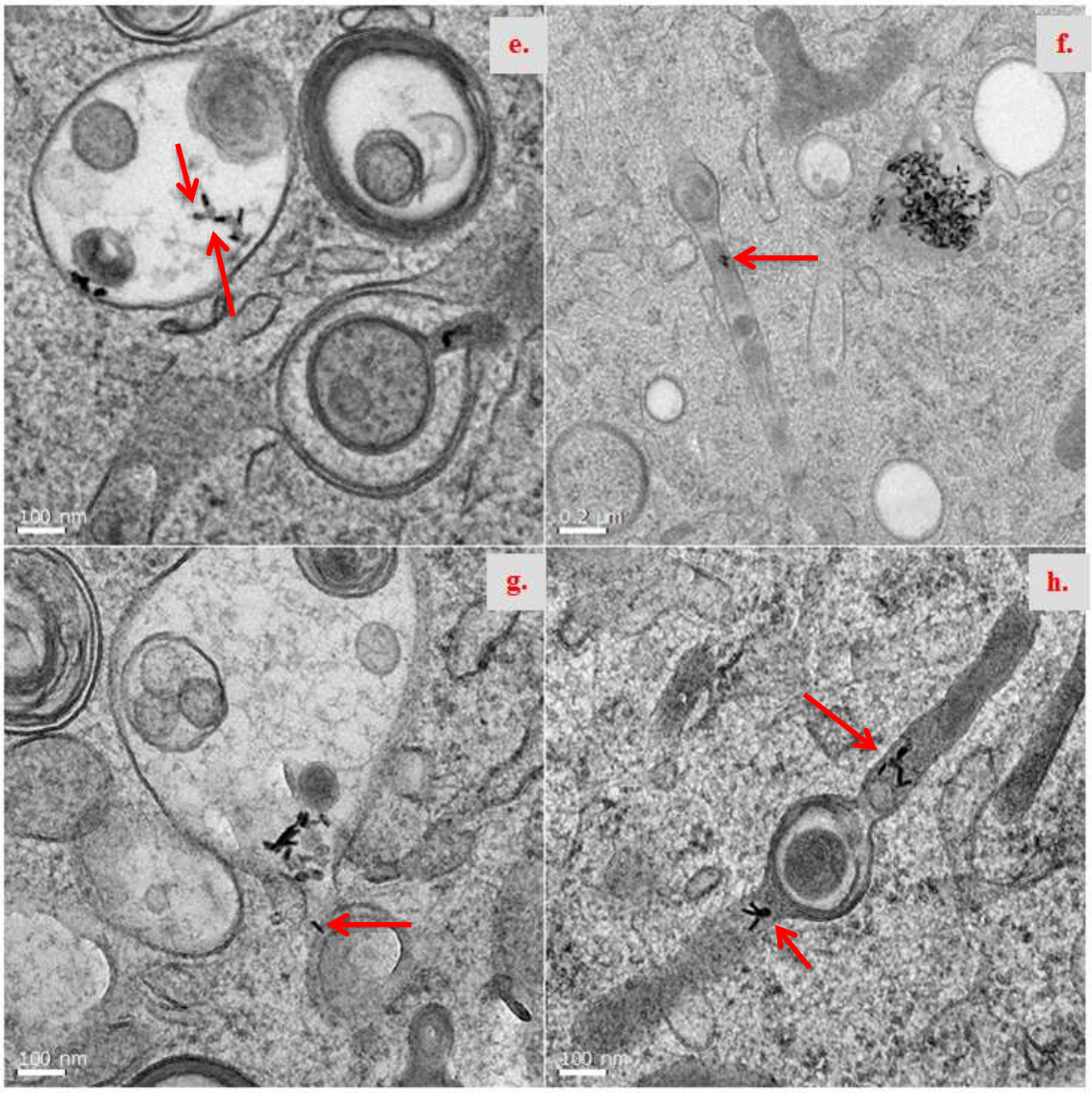

Figure 7 : TEM Images of the cellular uptake from HHA397 NPs with a concentration of 18,75 µg/mL for 24 hours ***e)*** *HHA397 NPs in RAW 264.7 cells in endosome/lysosome vesicles, scale 100 nm* ***f)*** *HHA397 NPs in RAW 264.7 cells in endosome/lysosome vesicles and the intracellular transport (indicated by arrows) of NPs with microtubules, scale 200 nm* ***g)*** *HHA397 NPs in RAW 264.7 cells endosome/lysosome vesicles, and endosomal/lysosomal escape(indicated by arrow, scale 100 nm* ***h)*** *HHA397 NPs in RAW 264.7, intracellular transport of NPs with microtubules, scale 100 nm*

As we can see in **Figure 6** and **Figure 7**, HHA397 quantum nanoplatelets have a very high electron dense and thus they can be identified easily in the intracellular environment. In the the RAW 264.7 cells they are found in large clusters. In addition, some of the observed NPs are found in a lower amount, only a few QNPs together, in vesicular structures. Considering the incubation time, it is likely that these are mostly lysosomes and not endosomes. From the TEM micrographs (**Figures 6 and 7)** we can

see that they are transported into the cell. For these experiments, mouse macrophages were used and due to their typical properties, we can say that the QNPs are taken up by a micropinocytosis process resulting in big clusters of intracellular NPs. Addionally, some of the NPs were separated and found in multivesicular endosomes in the cells. In **Figure 6.a** and in **Figure 6.c** the QNPs are found to be aggretated into big clusters however in **Figure 6.b** and **Figure 6.d** they are mostly 2-3 QNPs together and found either in large, vesicular structures (**Figure 6.d**) or without any surrounding membrane as individual particles in the cytosol (**Figure 6.b**). Before incubation to the cell the QNPs are diluted in cell media (DMEM) which contains FBS (Fetal Bovine Serum). Therefore, it can be assumed that the QNPs are covered by a protein corona before the uptake process. It can be speculated, that the areas indicated by arrows in **Figure 7.e** are the former protein corona of the QNPs. In **Figure 7.g** a QNP (and maybe more QNPs) seems to escape from an endosomal vesicle. However, it might also be the observation of an intracellular transport process. A similar observation can be done in **Figure 9.k**, where an similar kind of QNPs was incubated to a cell. A very unexpected observation is done in **Figure 7.f** and **Figure 7.h**, where a few QNPs are transported along or even within a microtubuli.

The cells were also checked before performing high pressure freezing by light microscope and I noticed for the incubation at a concentration of 75µg/mL QNPs, that many cells were no longer attached to the sapphire discs. Therefore, I deduced that a concentration of 75µg/mL of QNPs could be too high for the cells and they may be damaged and finally detach from the sapphire discs. I didn't observed the same effect for the RAW 264.7 cells, which were incubated QNPs at a concentration of 18,75µg/mL.

Figure 8 shows mainly the extracellular surrounding of a cell. Here are many exosome vesicles, which have QNPs inside and also probably protein corona (indicated by arrows). This image was taken after 1 hour incubation with 75µg/mL of QNPs.

From the examinations of this particular system it is not yet clear, if we can unambiguously identify the protein corona surrounding the QNPs by TEM. However, there are some morphological indications that the protein corona is still attached to the nanoparticles after the uptake process. Furthermore, even for the QNPs found in the exosomal structures, we found some indications of the presence of a protein corona.

However, a distinct identification of the protein corona solely by TEM observation is hardly possible.

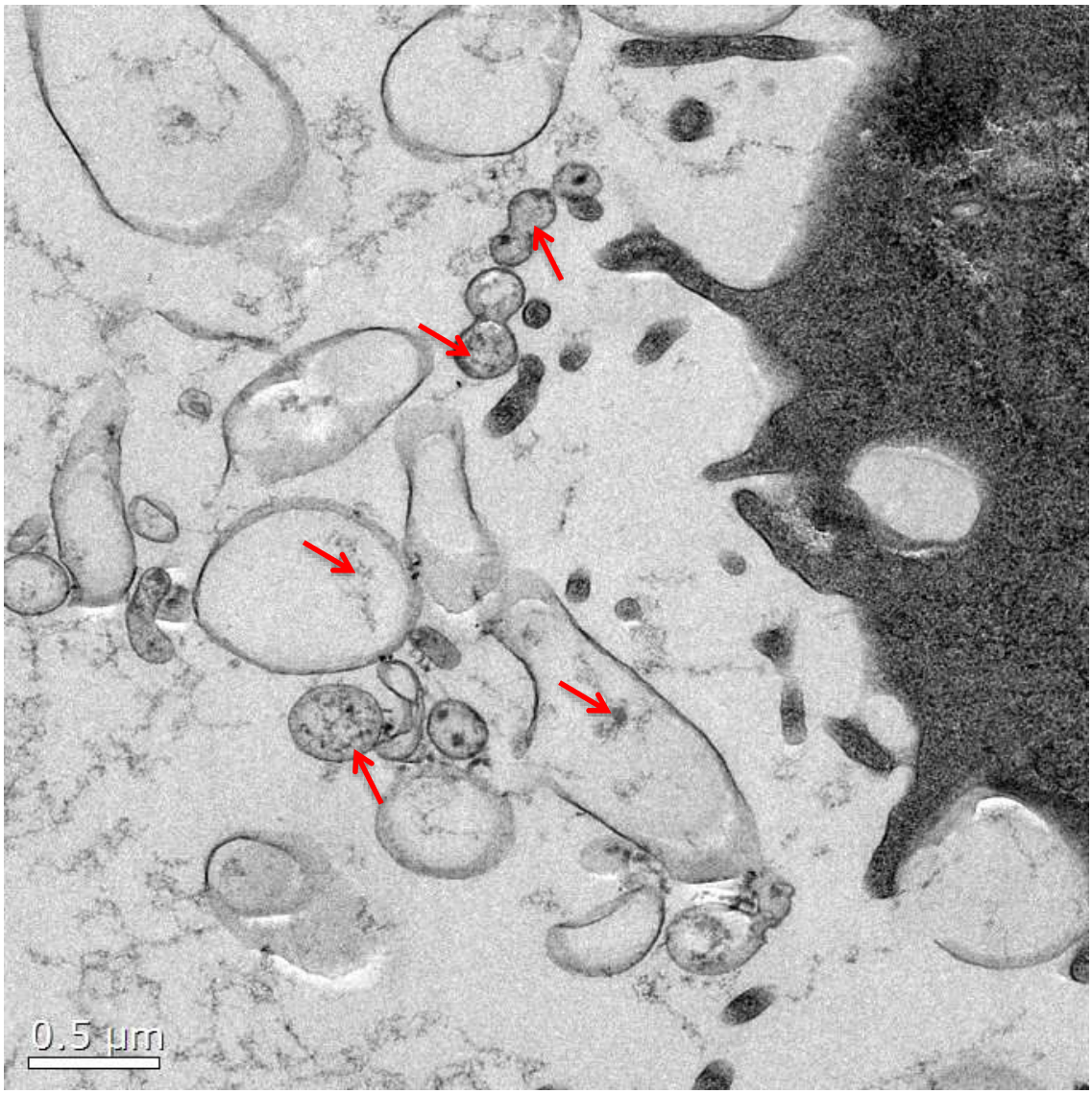

Figure 8: TEM Images of the cellular uptake and intercellular localization of HHA397 NPs with a concentration of 75µg/mL, for 1 h. *Exosome vesicles*

3.1.2 HHA296 Nanoplatelets (Henry Halim, MPIP)

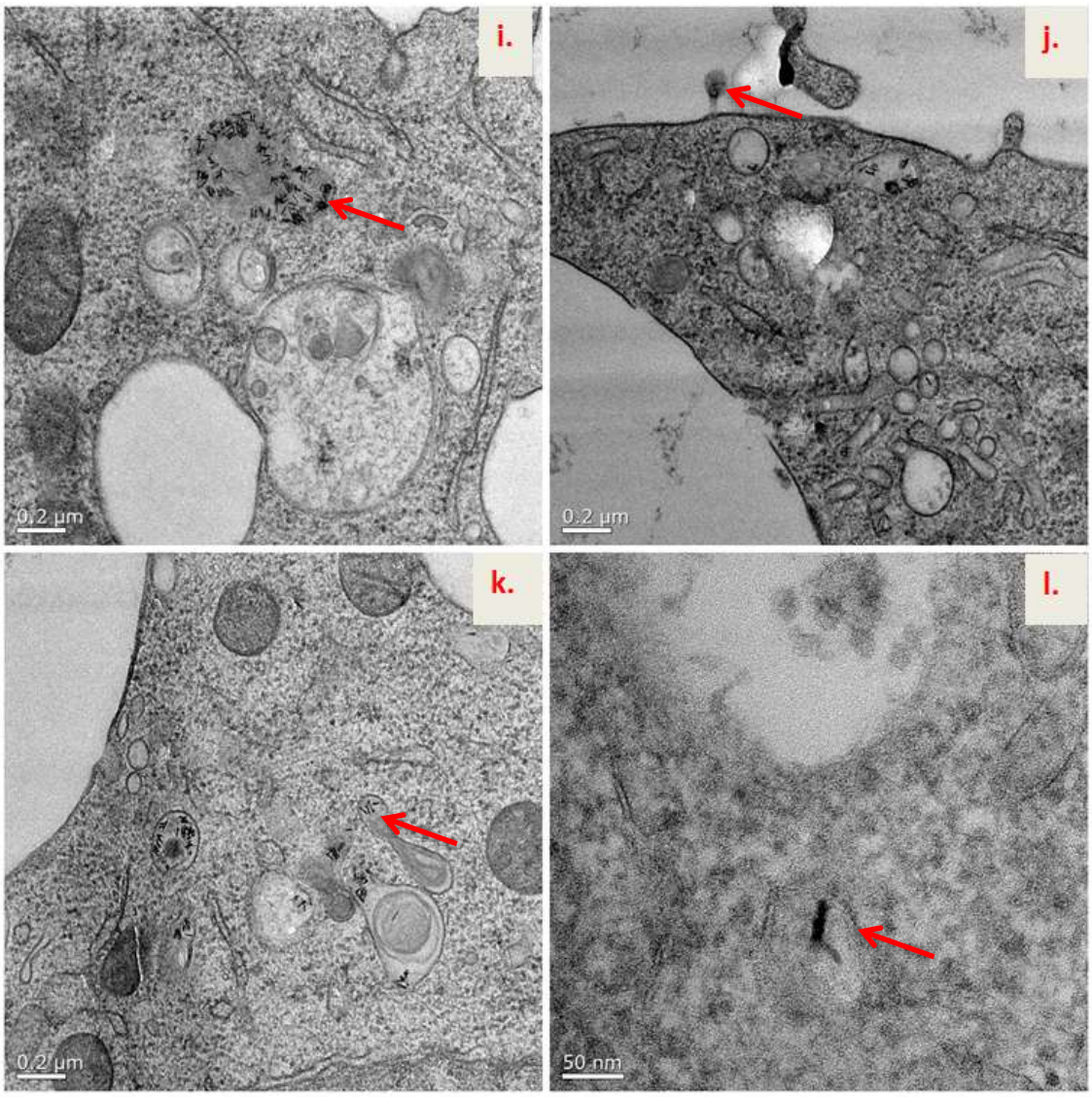

Figure 9 : TEM Images of the cellular uptake and intercellular localization of HHA296 NPs with a concentration of 75 µg/mL for 24 h (the cells were washed after 1 h with PBS and added fresh cell growth medium without NPs, and incubated for another 23 h ***i)*** *HHA296 NPs in RAW 264.7 cells in endosome vesicle, scale 200 nm* ***j)*** *Exocytosis of HHA296 NPs from RAW 264.7 cells, scale 200 nm* ***k)*** *HHA296 NPs in RAW 264.7 cells endosome vesicles, scale 200 nm* ***l)*** *A single HHA296 NP in cytosol RAW 264.7 cell, scale 50 nm*

The HHA296 QNPs showed very similar optical properties like HHA397 QPs. In contrast to the prior QNPs, these are coated with an additional polymer shell. However, as other QNPs they give strong contrast by TEM visualizing so it was very easy to detect them in the mouse macrophages, even though they are of very small size. Since the cell line used for this experiments (RAW 264.7) is a macrophage, it can be assumed that the uptake process is mainly macropinocytosis. Accordingly, the QNPs are most

likely taken up in big clusters. After 24 h incubation time, we detect them in clusters or as individual particles (**Figure 9.l)**. This shows, that by TEM visualization we can identify them even in small amounts. In the "**3.1.3 BSA Capsules + HH242 Quantum Platelets (Henry Halim, MPIP)"** part I will explain why it is important for the visualization by CLEM techniques. In **Figure 9.j** we can see the exocytosis of HHA296 QNPs very clearly. As mentioned before, they were uptaken in big clusters but we can see by exocytosis they are not in big clusters (**Figure 8** and **Figure 9.j**). So we can say that they are separated from each other during endosomal and exosomal pathway. However, despite the different surface chemistry of both the used QNPs, the morphological observations are similar. This might be indicative, that not the surface of the QNPs, but the adsorbed protein corona is dominating the uptake process of these particles.

3.2 Visualizing Intracellular Nanocapsules

3.2.1 BSA Capsules + HH242 Quantum Platelets (Henry Halim, MPIP)

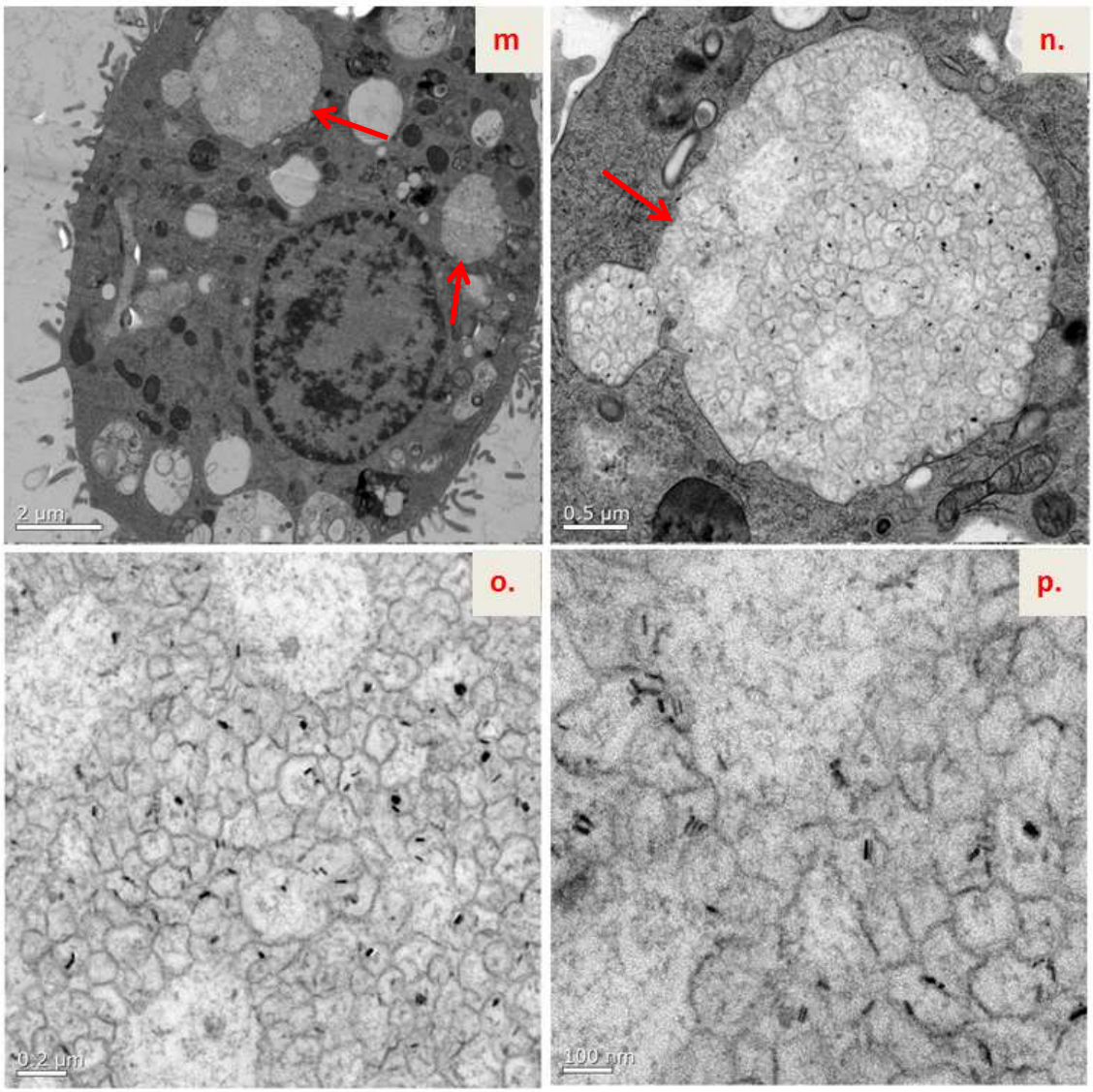

Figure 10: TEM Images of the cellular uptake and intercellular localization of BSA Capsules with HH242 quantum nanoplatelets with a concentration of 300 µg/mL for 24 h (the cells were washed after 1 h with PBS and added fresh cell growth medium without NPs, and incubated for 23 h ***m)*** *BSA Nanocapsules+ HH242 in RAW 264.7 cells in vesicles, scale 200 nm* ***n)*** *BSA Nanocapsules+ HH242 in RAW 264.7 cells, scale 500 nm* ***o)*** *BSA Nanocapsules+ HH242 in RAW 264.7 cells, scale 200 nm* ***p)*** *BSA Nanocapsules+ HH242 in RAW 264.7 cells, scale 100 nm*

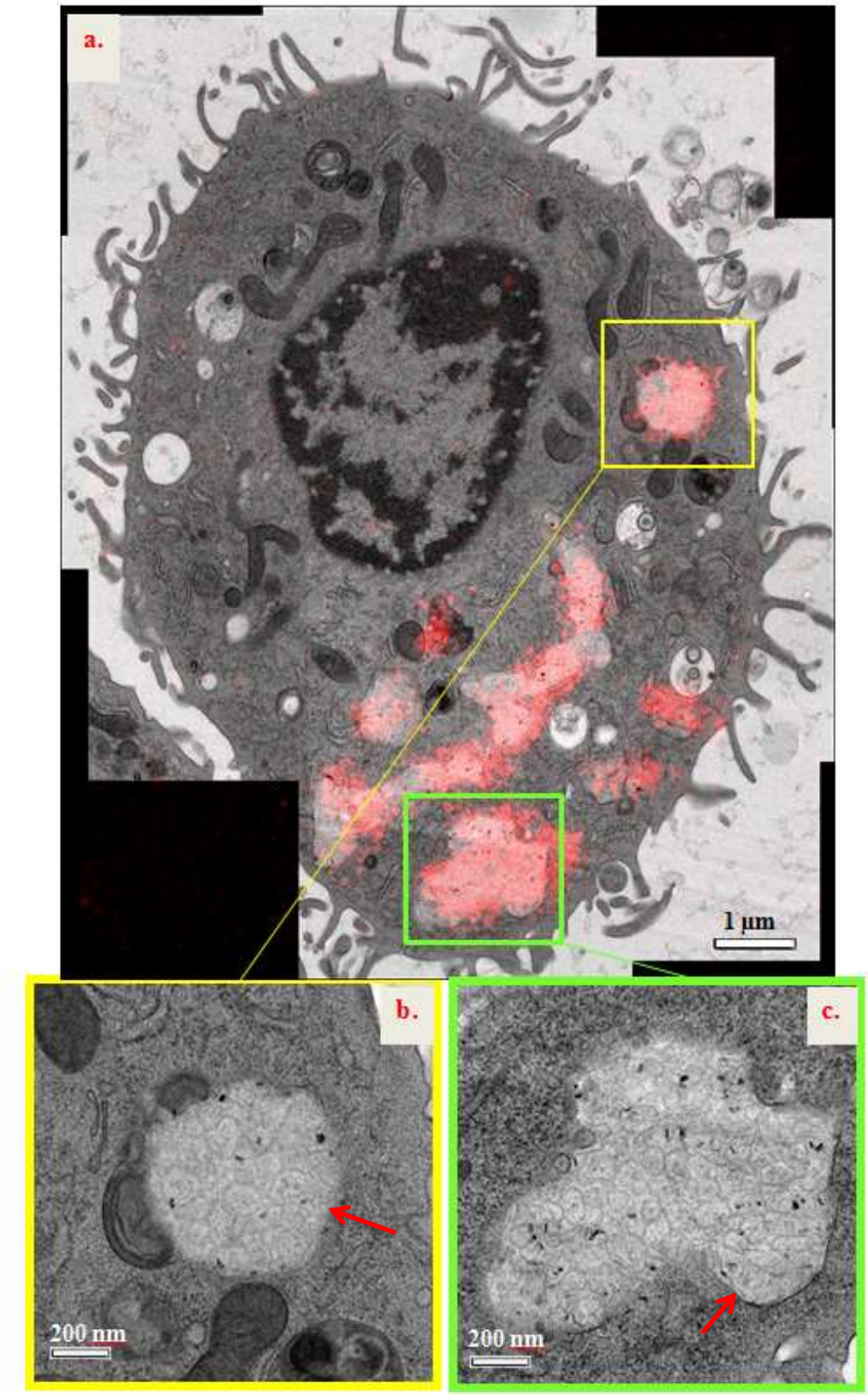

Figure 11: BSA nanocapsules + HH242 QNPs in RAW 264.7 cells ***a.)*** *CLEM Image (TEM and cLSM) of BSA Nanocapsules + HH242 (the BSA nanocapsules with a concentration of 300µg/mL and for 24 hours incubated with RAW 264.7 cells), scale bar 1µm* ***b.) & c.)*** *High magnification images of BSA nanocapsules + HH242 QNPs*

The BSA nanocapsules, like all protein nanocapsules, have some difficulties to be clearly identified by means of TEM visualization. The first reason is that they give very poor contrast to the surrounding, resin embedded cellular matrix. The second reason is, that they have very similar shape like other cell compartments. Therefore, distinctly distinguishing them from other cell structures without any marker or dye is impossible. We used QNPs for these BSA nanocapsules as marker and in this way thanks to the nanoplatelet, which are placed inside the BSA nanocapsules, they can be detected easily and unambiguously by means of TEM examination.

Another advantage of QNPs is their fluorescence. Many organic dyes lose their fluorescence after electron microscopy sample preparation process, but quantum platelets don't lose their fluorescence. In this way, CLEM technique can be also performed for these nanocapsules. Figure 11 shows the overlay of cLSM and SEM micrographs, where the fluorescence of the QNPs is displayed in red. Accordingly, the red overlay in the SEM micrograph clearly indicates the localization of QNPs and hence indirectly the BSA capsules as well. Although the BSA nanocapsules don't have too many QNPs inside (see **Figure 10.o** and **.p** and **Figure 11.a** and **.b**), the fluorescence of QNPs was quite satisfactory and easily detecable. Hence, with the QNP labeled BSA capsules we have a nanoparticle system which is highly suitable for unambiguous identification by TEM as well as by combined fluorescence and electron microscopical imaging.

As can be seen from **Figure 10 & 11**, the BSA nanocapsules were taken up in clusters into the cells and no individual QNPs (out of BSA nanocapsules) have been detected in the cytosol.

Although the high concentration (300µg/mL) of these BSA nanocapsules, the cells look very healthy by their appearance in the EM examination and we didn't see any cell apoptosis. In this way we can say that the BSA nanocapsules are not toxic for the cells.

The BSA nanocapsules with QNPs were visualized after 24 h incubation in very big clusters. This can happen in two ways; they could be taken up in big clusters by micropinocytosis and stayed in vesicles in clusters or they have been taken up one by one or in small clusters by other endocytotic processes, followed by an cellular controlled aggregation into these large agglomerates, as have been microscopically observed. Which of these two pathways is taken by the cell can´t be determined by the

experiments performed in this thesis. In order to determine the fate of the uptaken BSA nanocapsules by means of microstructural characterization by TEM or other CLEM related techniques, a series of different incubation times would have been necessary. By this way, a comprehensive illustration of the intracellular fate of the BSA nanocapsules can be reconstructed yielding information about the exact process leading to the very large clusters of intracellular BSA nanocapsules, found in this study. However, such an elaborate experimental work is outside the scope of this thesis and hence there is no information on the exact formation process leading to these large clusters of internalized nanparticles.

3.2.2 HES Nanocapsules + Cy5

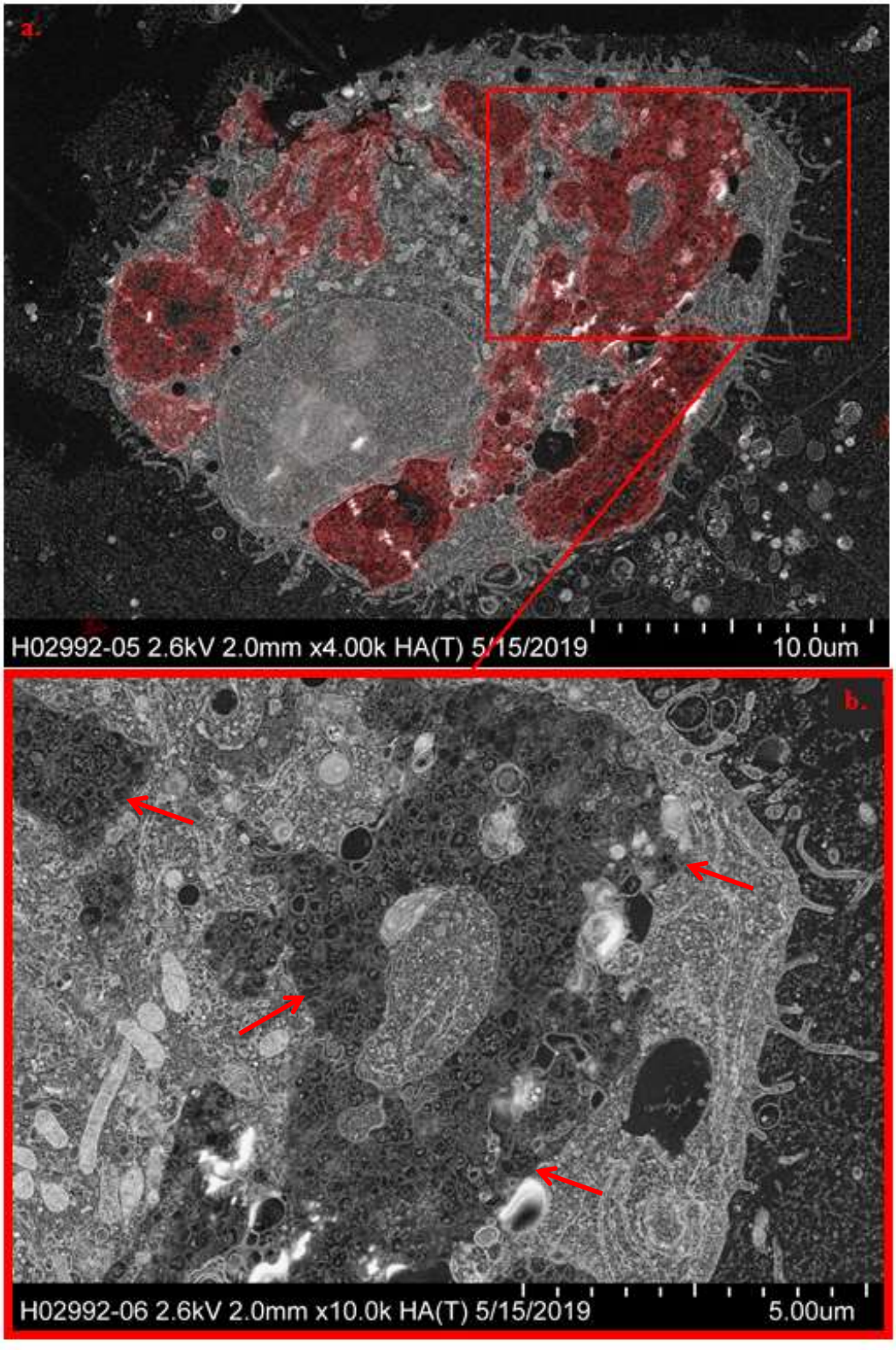

Figure 12: The HES nanocapsules + Cy5 with a concentration of 300 µg/mL in RAW 264.7 cell after 24 h incubation, ***a)*** *CLEM Image (SEM and cLSM) of HES Nanocapsules with Cy5, scale 10 um* ***b)*** *SEM image of HES capsules with higher magnification, scale 5 um*

Like for the BSA and other organic nanocapsules, the visualization of HES nanocapsules is difficult due to their low electron density difference to the surrounding matrix and due to their circular shape which can be found for many other cell compartments, making an unambiguous identification difficult.

Because of this reason, it was not possible to visualize these nanocapsules with a single microscopy method like TEM or SEM. Accordingly, a CLEM technique was applied, combining the advantages of fluorescence labelling and EM resolution.

In this case, the HES capsules did not contain any inorganic, fluorescent marker. However, Cy5 organic dye was used here for labeling the HES capsules. Usually, the problem using organic dyes in combination with the preparation for EM imaging is, that the organic dyes are known to lose their fluorescence due to the highly oxidizing reagents like OsO_4 used for staining the EM specimens. However, we managed to visualize the Cy5 labeled HES nanocapsules in thin sections prepared for SEM and using the very same section for cLSM imaging. It is not yet clear, why the Cy5 dye survived the preparation and this is a topic of ongoing research at the moment. Nonetheless, the fluorescence and EM micrographswere then overlaid to get a single image with fluorescence and also high resolution and magnification (**Figure 12**). Due to the identification via the Cy5 fluorescence it is now possible, to unambiguously identify the HES capsules in an EM micrograph.

Here we can also see the HES nanocapsules were taken up in very large clusters but the cell looks very healthy. It could be possible to dilute the nanocapsules, because the 300 µg/mL concentration is quite high but we have seen they are not toxic even for high concentration and 24 h incubation.

3.2.3 HRP Capsules + Cy5

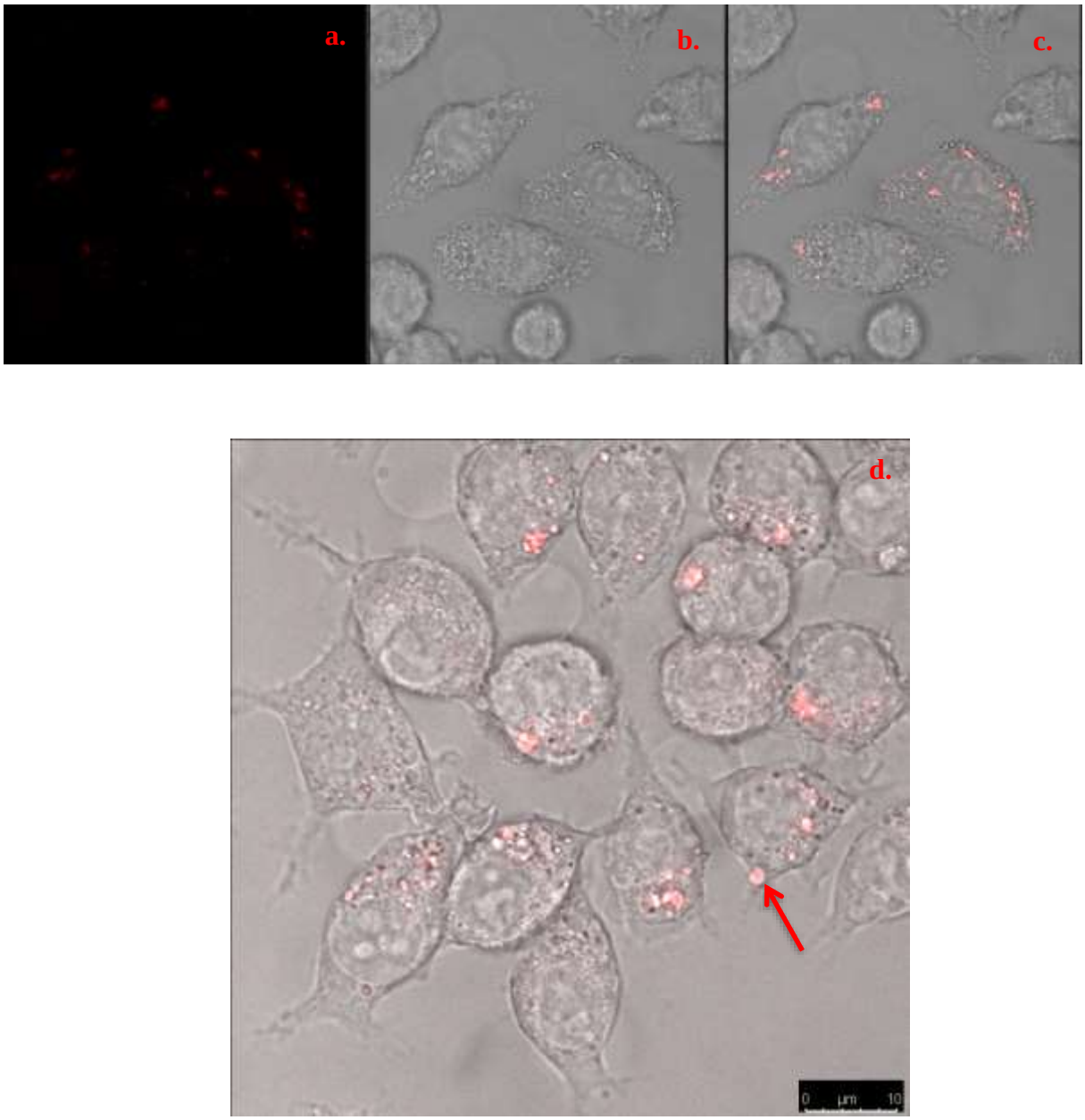

Figure 13: CSLM Images of intracellular visualization of HRP Capsules with Cy5 *(from Marina Machtakova)* in RAW 264.7 cells Concentration of HRP nanocapsules + Cy5 dye= 50 µg/mL, Time point=24h ***a.*** *Red Chanel for Cy5,* ***b.*** *Gray Scale Chanel,* ***c.*** *and* ***d.*** *Overlaid Chanels, scale 10 µm*

As we have seen in the last paragraphs, there are different strategies to prepare nanoparticle systems for microstructural characterization in the electron microscope. The main focus herein is, to unambiguously identify the nanoparticles in the cellular environment. As demonstrated for the HES and the BSA capsules, the incorporation of a fluorescent or high density marker into the polymeric nanoparticle / nanocapsule

facilitates CLEM and with that, their identification in the EM micrographs. In this sections, I will describe a slightly different approach using the chemical properties of a nanocapsule for identification purposes. HRP capsules are produced from horseradish peroxidase enzymes and in addition, they are labelled with Cy5 fluorescence dye. Normally, as mentioned before, protein nanocapsules are difficult to detect by TEM, because they do not have a different contrast. I scoped the problem of the low contrast of HRP nanocapsules in electron microscopy by applying 3,3'-diaminobenzidine (DAB) photoconversion and I aimed on correlating fluorescence and scanning electron microscopy images. DAB photoconversion is compatible with different cell embedding media after the precipitates have been formed. As such, e.g., epoxy resins after osmium post-fixation or acrylic resin without osmium post-fixation can be used. This approach represents a very promising tool, which will certainly provide more impact in the future.

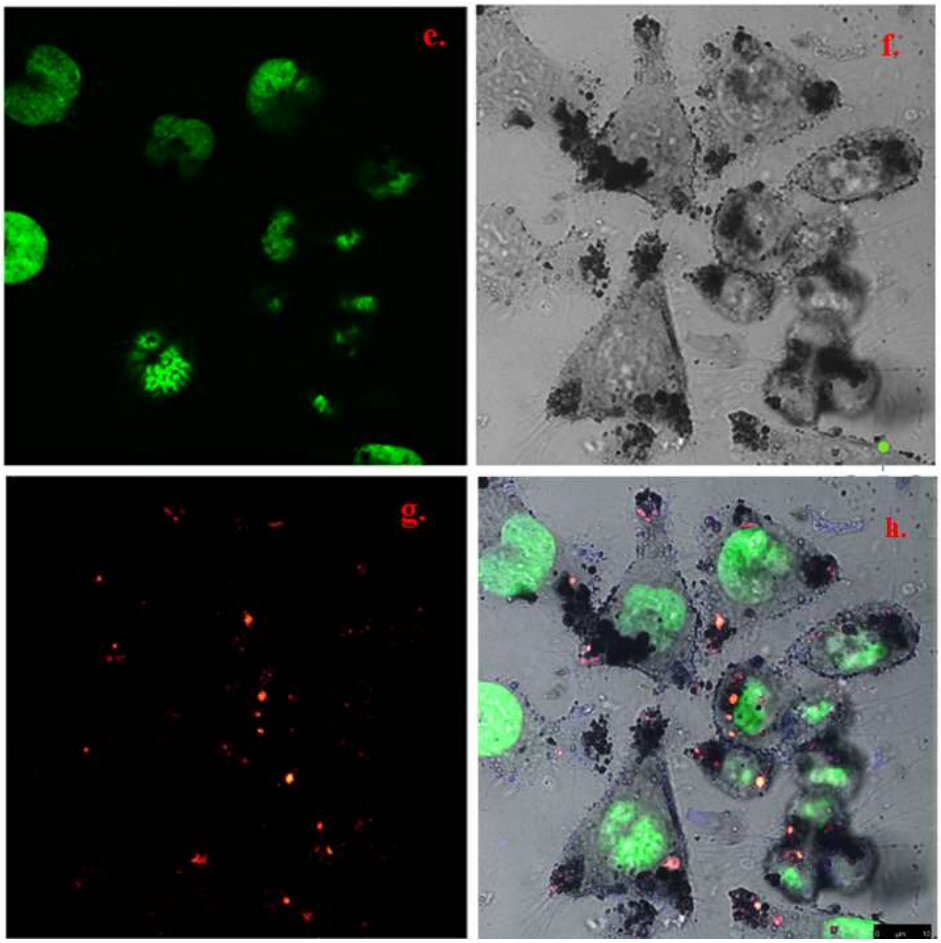

Figure 14: cLSM Images of DAB+H_2O_2 (with metal enhancer) stained HRP Capsules + *Cy5 (Marina Machtakova)* ***e.)*** *Chanel 1: For SYTOX Green Nucleus Staining* ***f.)*** *Chanel 2: Gray scale* ***g.)*** *Chanel 3: Cy5 stained HRP capsules* ***h.)*** *Overlaid all channels, scale bar 10 µm*

Firstly the HRP nanocapsules with Cy5 dye were visualized by cLSM (**Figure 13**) only to verify the DAB staining procedure before using it for CLEM. Due to fluorescence of Cy5 dye it was possible to detect the HRP capsules in the RAW 264.7 cells. Then DAB staining was applied. In **Figure 14;** after DAB staining process, the HRP nanocapsules are visualized by cLSM and there was a major difference. As we aspected, the HRP nanocapsules had become very strong black color. Unfortunetly, the DAB staining yields a very strong overstaining effect, which can be clearly seen in Figure 14.h. The area of the Cy5 signal is much smaller than the dark area resulting from the DAB staining procedure. At this point I can only speculate on the reason for the unsatisfactory result. It can be, that the staining kit used for this experiment was not compatible with one of the components.

In Figure 13 (unstained) we can partially recognize HRP capsules. It was difficult to detect all of them due to the low fluorescence intensity of Cy5 in the smaller capsules. However, the smallest and the largest of the DAB-stained HRP capsules can be detected very easily. In the cLSM images for some of the DAB stained HRP capsules (**Figure 14**), we can't see any red fluorescence, because the black color absorb the stimulation light.

The Cy5 labeled HRP nanocapsules (50µg/mL) were also incubated to RAW 264.7 cells

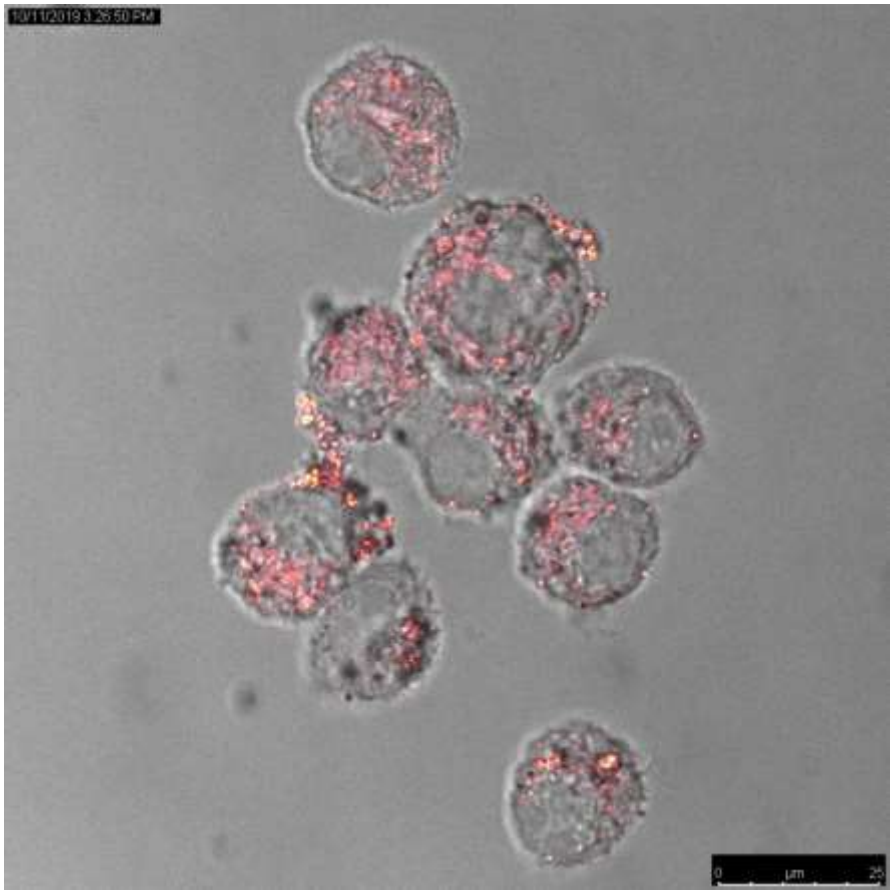

for 48 h and the HRP capsules can still be stained by DAB and the Cy5 dye is still in the HRP capsules. So we can see that there was no degradation of HRP capsules, if it had been, the capsule structure would have disintegrated and the dye would have leaked out of the capsules. Although the capsule structure is preserved here, the capsule structure does not looks to be very well preserved in the SEM image in **Figure 16**.

Figure 15: Incubation RAW 267.4 cells with a concentration of 50µg/mL of HRP nanocapsules for 48, *scale 25 µm* (In this image, the HRP nanocapsules were also stained with DAB+H_2O_2 but with other kind of DAB staining kit. This kit was not with metal enhancer, so their contrasts were not as strong as in **Figure 14**.)

After these processes and the proof of principle for DAB staining, RAW 264.7 cells were incubated with the Cy5 labelled HRP nanocapsules and stained with DAB staining kit (with metal enhancer). Then the cells were prepared using classic TEM sample preparation methods (HPF, FS, EPON embedding, sectioning) and finally the thin sections were visualized by SEM and cLSM. After that, the SEM and cLSM images were overlaid. From SEM image, the areas, where the HRP nanocapsules localized, were detected and were imaged again with SEM with a high magnification. The results are shown in **Figure 16**. The fluorescence signal of the Cy5 labeled HRP capsules has survived the EM sample preparation and yields the localization of the HRP capsules in the SEM micrograph. However, as can be seen in Figure 16.c, the contrast of the capsules has not been gained resulting a higher electron density, as it was usually reported for the HRP-DAB staining procedure [65]. In the SEM micrograph the HRP capsules are hardly to be recognized. The increase of electron density, as is expected for this kind of staining, is not observed for SEM imaging. The location of the HRP capsules should have gained a brighter contrast here, which is only very slightly visible. However, I have not inspected this sample in the TEM, where the effect of HRP-DAB staining is more visual.

Nonetheless, the CLEM technique using the fluorescence signal of the Cy5 labelled nanocapsules works for this system and one can see in **Figure 16.b** and **.c** that the HRP capsules are not really recognizable from their morphology. Compared to the BSA (**Figure 11**) and the HSA capsules (**Figure 12**) the HRP capsules already seem to be partly degraded since there is not recognizable capsule structure observable in the SEM micrographs.

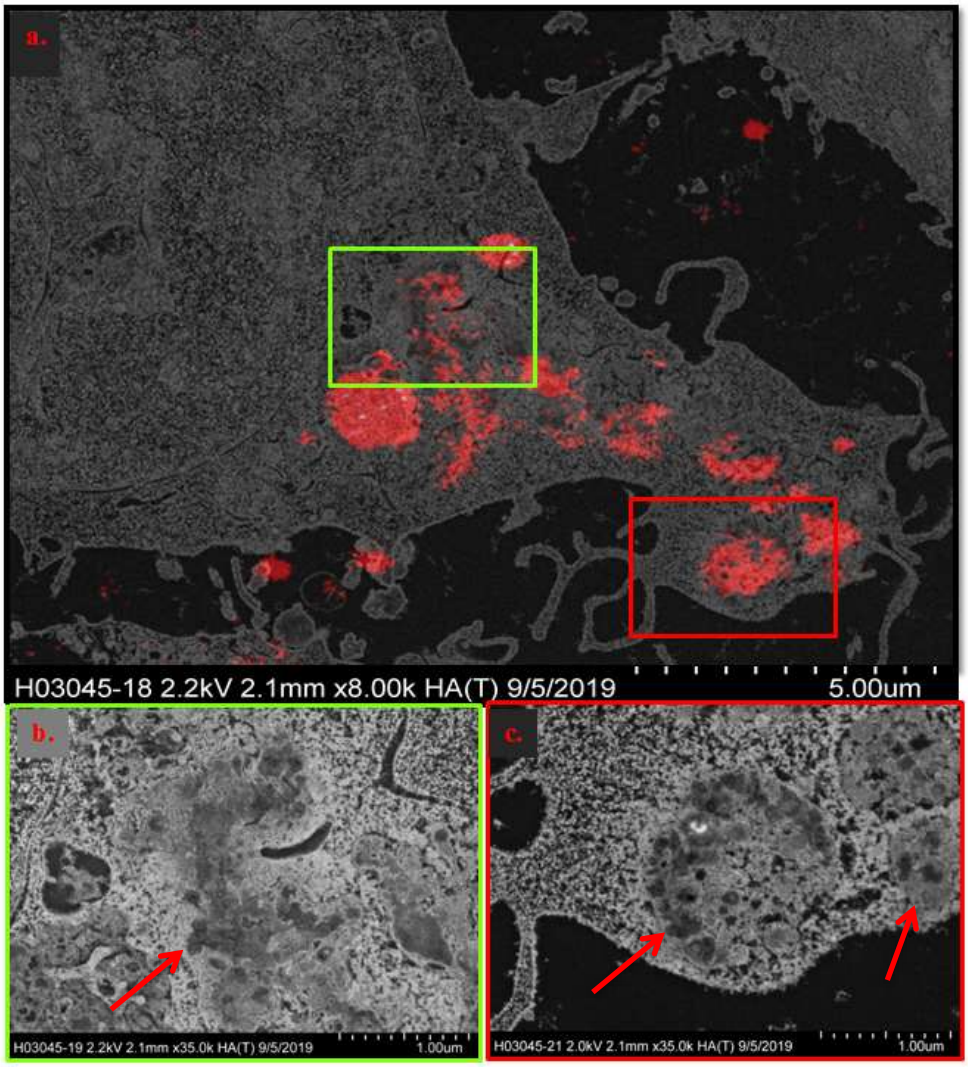

Figure 16: CLEM Images of HRP Capsules + Cy5 ***a.)*** *Overlaid SEM and cLSM Images of HRP Capsules + Cy5 in RAW 264.7 cell, scale 500 nm* ***b.****and* ***c.)*** *SEM Images of HRP Capsules with high magnification, scale 100 nm*

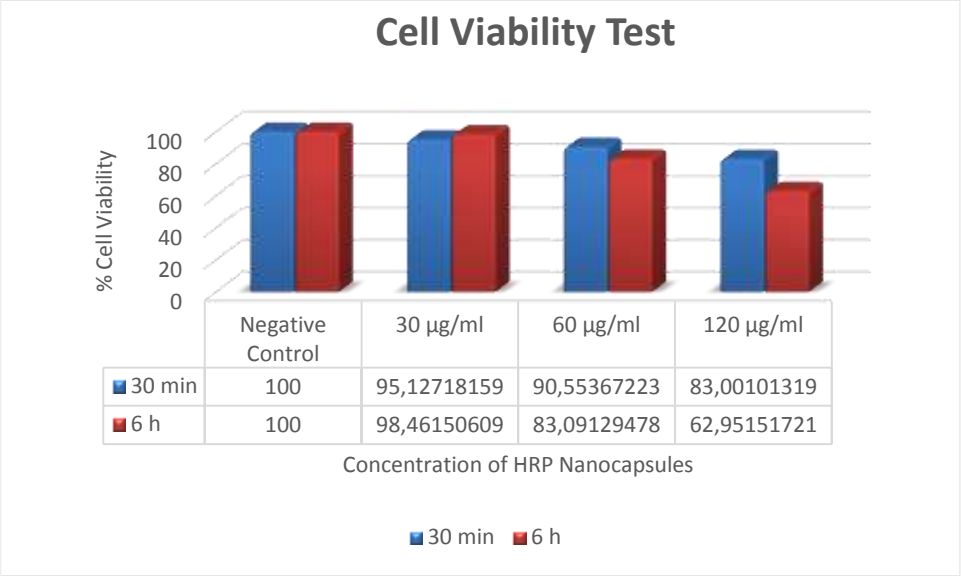

Diagramm 1: The CellTiter-Glo® Luminescent Cell Viability Assay Results

I also performed cell viability test to see the viability (Diagramm 1) after 6 h and 30 minutes with incubation with 30µg/mL, 60µg/mL and 120µg/mL of HRP nanocapsules. Predictably, the higher the capsule concentration, the lower the number of living cells, of course, as well as for the longer incubation time the results were similar. At the beginning, cell viability was 100%, after 30 minutes incubation with 30 µg/mL, the cell viability was 95 %; after 30 minutes incubation with 60µg/mL, the cell viability was 90 %, and after 30 minutes incubation with 120µg/mL HRP capsules, the cell viability was 83 %. After 6 h incubation with 30 µg/mL HRP nanocapsules the cell viability was 93 µg/mL, after 6 h incubation with 60 µg/mL the cell viability was decreased to 83 % and after 6 h incubation with 120 µg/mL the cell viability decreased rapidly to 62 %. This demonstrates, that the HRP nanocapsules are toxic, especially in high concentration and for a long incubation time.

3.3 Visualizing of Intracellular Polystyrene Nanoparticles + Cy5 labeled Protein corona

Protein corona studies are increasing. Information about the proteins surrounding the nanoparticles provides us information about the effect of the nanoparticle, as well as by examining the diversity of this protein to obtain information on many topics. An example is the use of protein corona in an early diagnosis test for cancer [64]. Therefore, it is of great importance to examine the protein corona. Furthermore, the protein corona formed when a nanoparticle come into contact with a biological environment, determines its biological behaviour.

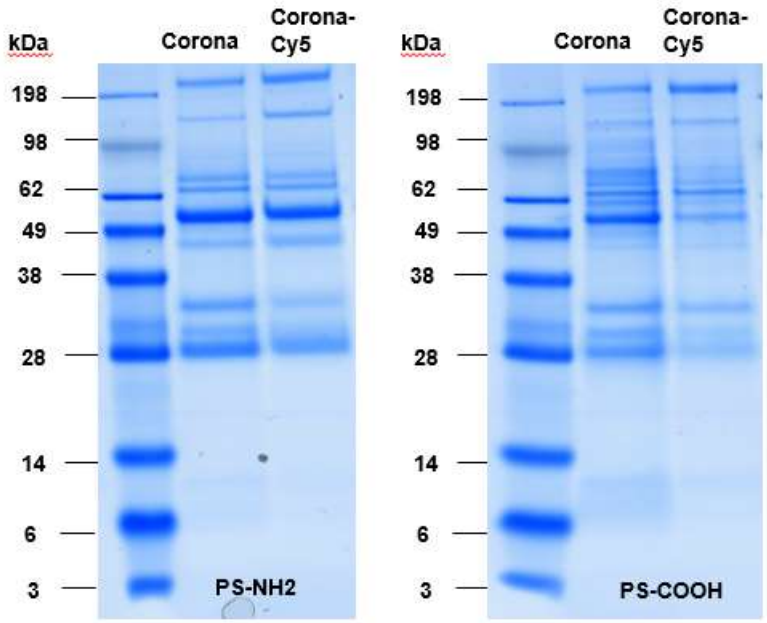

Figure 17: PS-NH2 and PS-COOH nanoparticles were incubated with mouse plasma or Cy5 labeled mouse plasma. The hard corona proteins were separated by SDS-PAGE and visualized by Coomassie Blue staining. There was no major difference in the protein pattern for mouse plasma or Cy5 labeled mouse plasma.

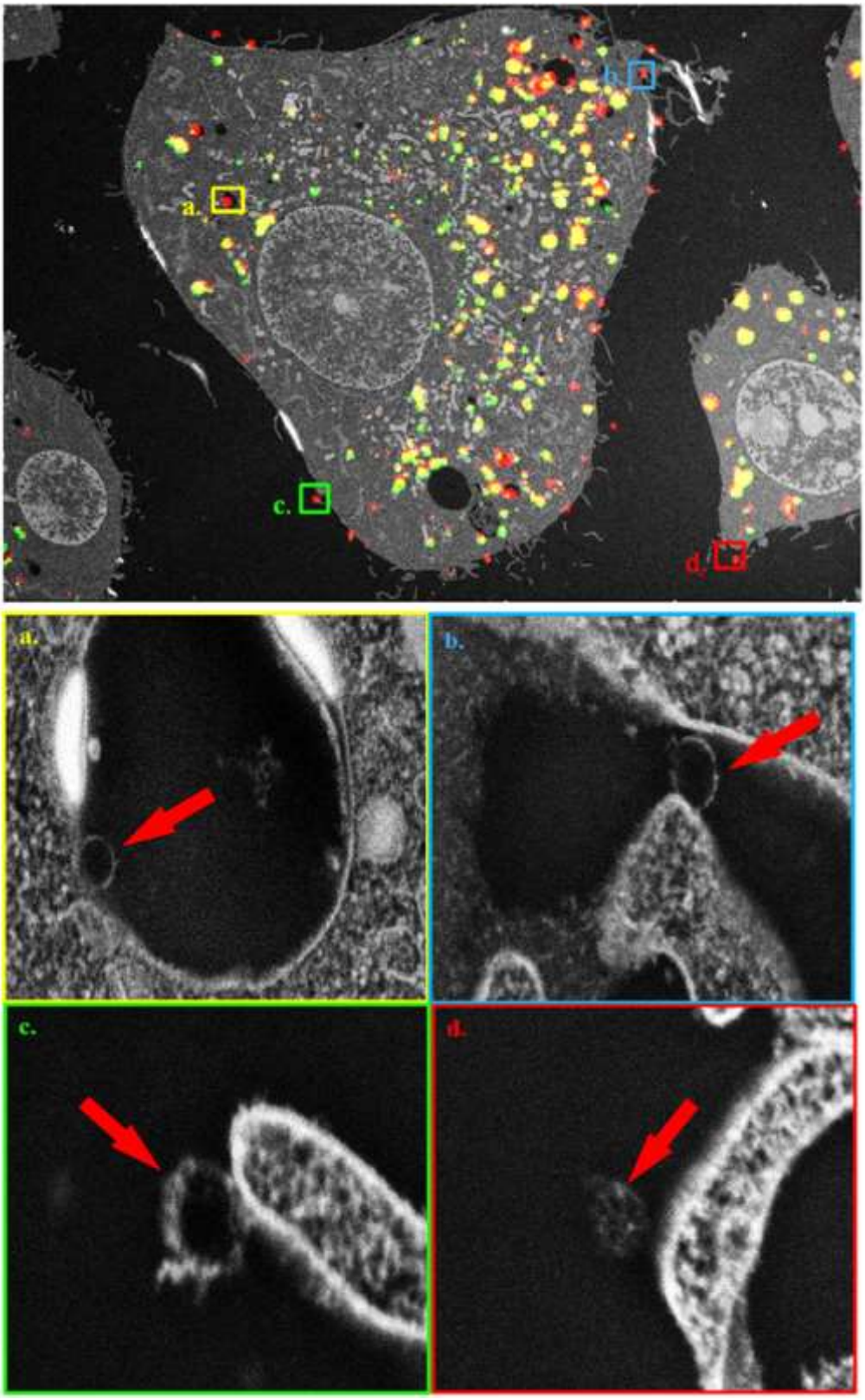

Figure 18: CLEM images (SEM and cLSM) of Cy5 labeled plasma corona and polystyrene nanoparticles (PS-NPs) *1.) Polystyrene Nanoparticles (Green fluorescence) 2.) Green: PS-NPs; Red: Cy5 labeled protein corona; Yellow: overlaid PS-NPs & Cy5 labeled protein corona. a., b., c., and d. are the ROI, where protein corona is placed; we can see them in more details in SEM images at higher magnification.*

For the microstructural characterization of the protein corona, I used PS-NPs (PS-COOH and PS-NH2) that were centrifuged together with Cy5-labelled Mouseplasma for 1 h at 37° C (~ 100 µl nanoparticle dispersion + 1 mL of Cy5 Mouseplasma; Centrifugation (30 min, 20.000 g); Resuspension ~ 100 µl of water). Afterwards, the protein coated PS nanoparticles were incubated to RAW 264.7 cells at a concentration of 300µg/mL for 2 hours. In the paper of Maria Kokkinopoulou et. al. [65] it was reported that IgG is a major component of the corona of PS-NH2 and COOH. For the Cy5-Mouseplasma an SDS-PAGE measurement was performed as well and visualized by Coomassie Blue staining. There was no major difference in the protein pattern for mouse plasma or Cy5 labeled mouse plasma (**Figure 17**). For the visualization of Cy5 labeled protein corona the CLEM technique was performed. The thin sections of the PS-NPs & Protein Corona + Cy5 samples were visualized by SEM and cLSM and the images were overlaid (**Figure 18**). This enabled us to detect the intracellular localization of the PS-NPs and Cy5-protein corona and to visualize them with high resolution. As we can see in the CLEM images, PS-NPs were surrounded by Cy5 labeled proteins. However, in some occasions we can detect individual protein coronas without any indication of the respective PS nanoparticle. This become evident in the area marked with an arrow in **Figure 18.a**. There is no fluorescence signal for the PS particle detectable, but the corona signal is clearly visible. When looking at this area in higher magnification, the morphology of the corona is preserved, but the corresponding NP is missing **(Figure 18.a**). The mechanism which leads to such an empty protein corona is not clear at all and needs in depth examination.

However, by the consequent application and development of correlative microscopy techniques I was able to visualize the protein corona and the corresponding nanoparticle. This development of a correlative method for the high resolution localization of intracellular nanoparticles and their protein corona may finally help to understand the nanoparticle-cell interaction and yield new insights to facilitate nanoparticle-based medical therapies.

4. Conclusion

In this master thesis, inorganic as well as organic nanoparticles were visualized intracellular by applying different methods. In conclusion, inorganic nanoparticles like

quantum nanoplatelets could be used for many imaging tools. Because as the results are supported, they have very rich contrast. They could be used as a marker for other nanoparticles like the example BSA protein nanocapsules.

Organic nanoparticles have some difficulties by visualizing. They have very low electron dense and similar shape with other cell parts. So it is necessary to give them some properties such as bright fluorescence and strong contrast and also CLEM technique is required. For example, by using Cy5 organic dye, HES nanocapsules enhanced bright red fluorescence. Cy5 organic dye was preferred because many organic dyes after electron microscopy sample preparation can't survive, but Cy5 organic dye still has fluorescence after the EM sample processing. Therefore I also used this dye to visualize protein corona. To visualize the BSA nanocapsules, quantum platelets were used. That have 2 advantages; they have strong contrast so it was very easy to detect them in the cell and QNP have also florescence, in this way I also performed CLEM technique. To visualize HRP nanocapsules, as we also know from DAB-HRP detection kits, which commonly used in biochemical applications, DAB staining was performed. When HRP interact with DAB and hydrogen peroxidase, it gives a brown-black product (oxidased DAB) and water. This reaction allows us to detect the HRP nanocapsules easily. The HRP nanocapsules have inside Cy5 dye but EM has only gray scale so it doesn't help to visualizing by EM. But after DAB staining, they got more contrast so it was easier to identify the HRP nanocapsules by SEM visualizing.

As a result of my work I have seen that the CLEM technique is very successful in many different types of nanoparticles, especially this technique was definitely required for the visualizing intracellular organic nanoparticles and protein corona.

5. Acknowledgements

Throughout the writing of this dissertation I have received a great deal of support and assistance. I would first like to thank my supervisors, Prof. Dr. Katharina Landfester, and Dr. Ingo Lieberwirth, whose expertise was invaluable in the formulating of the research topic and methodology in particular.

I also want to thank to thank to Prof. Dr. Thomas Hankeln for agreeing to be my second supervisor.

I would like to acknowledge my colleagues at MPIP for their wonderful collaboration. You supported me greatly and were always willing to help me. I would particularly like to single out Shen Han and Dr. Johanna Simon. I want to thank you for your support and excellent cooperation. I would also like to thank Dr. Anke Kaltbeitzel and Christoph Sieber, for helping me whenever I need it and to Henry Halim, Marina Machtakova and Marie-Luise Frey to preparing nanoparticles and nanocapsules, which I used during my master thesis study.

I would like to thank the Max Planck Society for providing excellent working conditions and for its financial support.

I dedicate this master thesis to my father Arif Yangazoglu, who passed away in 2009, and to my lovely mother Münevver Yangazoglu and I would like to express my wholehearted thanks for all their sacrifices and support. In addition, special thanks to my siblings who have always been with me. I am very lucky to have such a family.

6. References

1. Bregar VB, Lojk J, Suštar V, Veranič P, Pavlin M. Visualization of internalization of functionalized cobalt ferrite nanoparticles and their intracellular fate. Int J Nanomedicine. 2013;8:919–931. doi:10.2147/IJN.S38749
2. Mahapatro A, Singh DK. Biodegradable nanoparticles are excellent vehicle for site directed in-vivo delivery of drugs and vaccines. J Nanobiotechnology. 2011;9(1):55. [PMC free article] [PubMed] [Google Scholar]
3. Qi LF, Xu ZR, Li Y, Jiang X, Han XY. In vitro effects of chitosan nanoparticles on proliferation of human gastric carcinoma cell line MGC803 cells. World J Gastroenterol. 2005;11(33):5136–5141. [PMC free article] [PubMed] [Google Scholar]
4. Berry CC, Wells S, Charles S, Aitchison G, Curtis AS. Cell response to dextran-derivatised iron oxide nanoparticles post internalisation. Biomaterials. 2004;25(23):5405–5413. [PubMed] [Google Scholar]
5. Kim JS, Yoon TJ, Yu KN, et al. Cellular uptake of magnetic nanoparticle is mediated through energy-dependent endocytosis in A549 cells. J Vet Sci. 2006;7(4):321–326. [PMC free article] [PubMed] [Google Scholar]
6. Shukla R, Bansal V, Chaudhary M, Basu A, Bhonde RR, Sastry M. Biocompatibility of gold nanoparticles and their endocytotic fate inside the cellular compartment: a microscopic overview. Langmuir. 2005;21(23):10644–10654.
7. Yen HJ, Hsu SH, Tsai CL. Cytotoxicity and immunological response of gold and silver nanoparticles of different sizes. Small. 2009;5(13):1553–1561. [PubMed] [Google Scholar]
8. Nam HY, Kwon SM, Chung H, et al. Cellular uptake mechanism and intracellular fate of hydrophobically modified glycol chitosan nanoparticles. J Control Release. 2009;135(3):259–267. [PubMed] [Google Scholar]
9. Asharani PV, Hande MP, Valiyaveettil S. Anti-proliferative activity of silver nanoparticles. BMC Cell Biol. 2009;10:65. [PMC free article] [PubMed] [Google Scholar]
10. Buzea, Cristina; Pacheco, Ivan; Robbie, Kevin (2007). "Nanomaterials and Nanoparticles: Sources and Toxicity". Biointerphases. 2 (4): MR17–MR71. arXiv:0801.3280. doi:10.1116/1.2815690. PMID 20419892

11. David J. Mc Carthy&Meenakshi Malhotra&Aoife M. O'Mahony&John F. Cryan&Caitriona M. O'DriscollReceived: 17 July 2014 /Accepted: 6 October 2014#Springer Science+Business Media New York 2014. Pharm Res DOI 10.1007/s11095-014-1545-6

12. Jeevanandam J, Barhoum A, Chan YS, Dufresne A, Danquah MK. Review on nanoparticles and nanostructured materials: history, sources, toxicity and regulations. Beilstein J Nanotechnol. 2018;9:1050–1074. Published 2018 Apr 3. doi:10.3762/bjnano.9.98

13. Martin Reifarth, Ulrich S. Schubert, and Stephanie Hoeppener. Considerations for the Uptake Characteristics of Inorganic Nanoparticles into Mammalian Cells – Insights Gained by TEM Investigations. DOI: 10.1002/adbi.201700254

14. S. Salatin, S. Maleki Dizaj, A. Yari Khosroushahi, Cell Biol. Int. 2015, 39, 881.

15. L. Shang, K. Nienhaus, G. U. Nienhaus, J. Nanobiotechnol. 2014, 12, 5.

16. C. Kinnear, T. L. Moore, L. Rodriguez-Lorenzo, B. Rothen-Ruthishauser, A. Petri-Fink, Chem. Rev. 2017, 117, 11476.

17. A. Albanase, W. C. W. Chan, ACS Nano 2011, 5, 5478.

18. E. Fröhlich, Int. J. Nanomed. 2012, 7, 5577.

19. E. I. Ryabchikova, N. A. Mazurkova, N. V. Shikina, Z. R. Ismagilov, J. Med. Chem. Biol. Radiol. Def. 2010, 8, pp. 1-18.

20. M. A. Maurer-Jones, Y.-S. Lin, C. L. Haynes, ACS Nano 2010, 4, 3363.

21. C. Gitrowski, A. R. Al-Jubory, R. D. Handy, Toxicol. Lett. 2014, 226, 264.

22. D. Docter, D. Westmeier, M. Markiewicz, S. Stolte, S. K. Knauer, R. H. Stauber, Chem. Soc. Rev. 2015, 44, 6094.

23. I. George, G. Naudin, S. Boland, S. Mornet, V. Contremoulins, K. Beugnon, L. Martinon, O. Lambert, A. Baeza-Squiban, Nanoscale 2015, 7, 4529.

24. J. F. Hillyer, R. M. Albrecht, J. Pharm. Sci. 2001, 90, 1927.

25. K. O. Yu, C. M. Grabinski, A. M. Schrand, R. C. Murdock, W. Wang, B. Gu, J. J. Schlager, S. M. Hussain, J. Nanopart. Res. 2009, 11, 15.

26. D. Docter, D. Westmeier, M. Markiewicz, S. Stolte, S. K. Knauer, R. H. Stauber, Chem. Soc. Rev. 2015, 44, 6094.

27. V. H. Nguyen, B.-J. Lee, Int. J. Nanomed. 2017, 12, 3137.

28. C. Corbo, R. Molinaro, A. Parodi, N. E. Toledano Furman, F. Salvatore, E. Tasciotti, Nanomedicine 2016, 11, 81.

29. Martin Reifarth, Ulrich S. Schubert, Stephanie Hoeppener First published: 20 June 2018 https://doi.org/10.1002/adbi.201700254

30. D. Mahl, C. Greulich, W. Meyer-Zaika, M. Koller, M. Epple, J. Mater. Chem. 2010, 20, 6176.

31. J. Park, J.-H. Park, K.-S. Ock, E.-O. Ganbold, N. W. Song, K. Cho, S. Y. Lee, S.-W. Joo, J. Colloid Interface Sci. 2011, 363, 105.

32. A. K. Murthy, R. J. Stover, W. G. Hardin, R. Schramm, G. D. Nie, S. Gourisankar, T. M. Truskett, K. V. Sokolov, K. P. Johnston, J. Am. Chem. Soc. 2013, 135, 7799.

33. C. T. Ng, F. M. A. Tang, J. J. e. Li, C. Ong, L. L. Y. Yung, B. H. Bay, Anat. Rec. 2015, 298, 418.

34. Hemant K.S. Yadav, Manar S. Debe, in Nanocarriers for Drug Delivery, 2019

35. F. Masood, Mater. Sci. Eng. C2016, 60, 569; T. Patel, J. M. Piepmeier, W. M. Saltzman, Adv. Drug Delivery Rev. 2012, 64, 701; M. Elsabahy, K. L. Wooley, Chem. Soc. Rev. 2012, 41, 2545.

36. Chan J.M., Valencia P.M., Zhang L., Langer R., Farokhzad O.C. (2010) Polymeric Nanoparticles for Drug Delivery. In: Grobmyer S., Moudgil B. (eds) Cancer Nanotechnology. Methods in Molecular Biology (Methods and Protocols), vol 624. Humana Press PMID: 20217595 DOI:10.1007/978-1-60761-609-2_11

37. AnjaliJoshi, Amrit PalToor, GauravVerma Panjab University, Chandigarh, India Massachusetts Institute of Technology, Cambridge, MA, United States 2017 https://doi.org/10.1016/B978-0-323-46143-6.00027-0

38. C. Ng, J. Li, R. Perumalsamy, F. Watt, L. Yung, B.Bay, Microsc. Sci. Technol. Appl. Educ. 2010, 1, 316.

39. A. Musyanovych, J. Dausend, M. Dass, P. Walther, V. Mailänder, K. Landfester, Acta Biomater. 2011, 7, 4160.

40. A. Tautzenberger, L. Kreja, A. Zeller, S. Lorenz, H. Schrezenmeier, V. Mailänder, K. Landfester, A. Ignatius, Biomaterials 2011, 32, 1706.

41. Baier, G.; Musyanovych, A.; Dass, M.; Theisinger, S.; Landfester, K. Biomacromolecules 2010, 11 (4) 960– 968 [ACS Full Text], [CAS]

42. Haass, A.; Treib, J.; Pindur, G.; Krack, P.; Wenzel, E.; Schimrigk, K. Naunyn-Schmiedeberg's Arch. Pharmacol. 1989, 339

43. Kiesewetter, H.; Erlenwein, S.; Jung, F.; Wenzel, E.; Vogel, W.; Dyckmans, J.; Bach, R.; Hahmann, H.; Schieffer, H.; Bette, L. Klin. Wochenschr. 1988, 66

44. Kiesewetter, H.; Jung, F.; Blume, J.; Gerhards, M. Klin. Wochenschr. 1987, 65 (7) 324– 330[Crossref], [PubMed], [CAS], Google Scholar

45. Devy, J.; Balasse, E.; Kaplan, H.; Madoulet, C.; Andry, M.-C. International Journal of Pharmaceutics (2006), 307 (2), 194-200CODEN: IJPHDE; ISSN:0378-5173. (Elsevier Ltd.)).

46. Hayat M (1987) Correlative microscopy in biology. In Hayat MA, ed. Instrumentation and Methods. London, Academic Press.

47. Juette MF, Gould TJ, Lessard MD, Mlodzianoski MJ, Nagpure BS, Bennett BT, Hess ST, Bewersdorf J. Three-dimensional sub–100 nm resolution fluorescence microscopy of thick samples. Nature methods. 2008;5:527–529.

48. Rong Sun, Yun-Tao Liu, Chang-Lu Tao, Lei Qi, Pak-Ming Lau, Z. Hong Zhou and Guo-Qiang Bi, Biophys Rep, 2019, 5, 111 DOI: 10.1007/s41048-019-0092-4

49. Sei Saitoh; Department of Anatomy II and Cell Biology, Fujita Health University School of Medicine, Toyoake, Japan. DOI: 10.5772/intechopen.81716

50. J. Mater. Chem. B. 2014, 2, 2060. DOI: 10.1039/c3tb21526a. Nanoparticle-Protein Corona Complexes Govern the Biological Fates and Functions of Nanoparticles

51. Nguyen VH, Lee BJ. Protein corona: a new approach for nanomedicine design. Int J Nanomedicine. 2017;12:3137–3151. Published 2017 Apr 18. doi:10.2147/IJN.S129300.

52. T. Cedervall, I. Lynch, M.Foy, T. Berggard, S. C. Donnelly, G. Cagney, S. Linse and K. A. Dawson, Angrew. Chem., Int. Ed., 2007, 46, 5754-5756. #### M. Lundqvist, J. Stigler, G. Elia, I. Lynch, T. Cedervall and K. A. Dawson, Proc. Natl. Acad. Sci. U. S. A., 2008, 105, 14265-14270.

53. Nanoparticle-Protein Corona Complexes Govern the Biological Fates and Functions of Nanoparticles. Available from: https://www.researchgate.net/publication/261064550_Nanoparticle-Protein_Corona_Complexes_Govern_the_Biological_Fates_and_Functions_of_Nanoparticles [accessed Oct 02 2019].

54. Walkey, C. D. and W. C. Chan (2012). "Understanding and controlling the interaction of nanomaterials with proteins in a physiological environment." Chemical Society Reviews 41(7): 2780-2799

55. Nguyen VH, Lee BJ. Protein corona: a new approach for nanomedicine design. Int J Nanomedicine. 2017;12:3137–3151. Published 2017 Apr 18. doi:10.2147/IJN.S129300

56. Tenzer, S., et al. (2013). "Rapid formation of plasma protein corona critically affects nanoparticle pathophysiology." Nature nanotechnology8(10): 772-781.

57. Lundqvist, Stigler et al. 2008, Ehrenberg, Friedman et al. 2009, Guarnieri, Guaccio et al. 2011, Lesniak, Fenaroli et al. 2012.

58. Owens, D. E. and N. A. Peppas (2006). "Opsonization, biodistribution, and pharmacokinetics of polymeric nanoparticles." International journal of pharmaceutics 307(1): 93-102.

59. Runa, S., et al. (2014). PEGylated nanoparticles: protein corona and secondary structure. SPIE NanoScience+ Engineering, International Society for Optics and Photonics.

60. Winkelstein, J. A. (1973). "Opsonins: their function, identity, and clinical significance." The Journal of pediatrics82(5): 747-753.

61. Illum, Davis et al. 1987, Owens and Peppas 2006, Gref, Domb et al. 2012.

62. Wolf, T., et al. (2015). "A Library of Well-Defined and Water-Soluble Poly (alkyl phosphonate) s with Adjustable Hydrolysis." Macromolecules48(12): 3853-3863.

63. D. Caputo, M. Papi, R. Coppola, S. Palchetti, L. Digiacomo, G. Caracciolo and D. Pozzi. Nanoscale, 2017, 9, 349

64. Corbo C, Molinaro R, Parodi A, Toledano Furman NE, Salvatore F, Tasciotti E. The impact of nanoparticle protein corona on cytotoxicity, immunotoxicity and target drug delivery. Nanomedicine (Lond). 2016;11(1):81–100. doi:10.2217/nnm.15.188

65. Jianli Li, Yue Wang, Shu-Ling Chiu and Hollis T. Cline, Front. Neural Circuits, 2010, 4, doi:10.3389/neuro.04.006.2010

66. Maria Kokkinopoulou, Johanna Simon, Katharina Landfester, Volker Mailänder and Ingo Lieberwirth, Nanoscale, 2017, 9, 8858-8870